JOURNAL OF MATERIALS SCIENCE 11 (1976) 2105–2141

Review

The physical properties of composite materials

D. K. HALE
Division of Chemical Standards, National Physical Laboratory, Teddington, Middlesex, UK

In this review, the physical properties of composite materials are discussed; however, discussion of the mechanical properties has been excluded except when necessary for the consideration of properties such as thermal expansion or swelling and shrinkage. One of the main aims in the review has been to show how the theoretical and experimental information that is already available may be used (a) to design and construct composite materials with predetermined physical properties and (b) to ensure that the physical properties of composite materials are properly measured and properly defined.

1. Introduction

The outstanding mechanical properties of fibre composites and especially the unique combinations of low density with high strength and stiffness which can be achieved with these materials, have led not only to extensive research on the mechanical properties of composites, but also to a highly developed technology. In comparison, relatively little effort has been devoted to the other physical properties of composites. Properties such as thermal and electrical conductivity, thermal expansion, swelling and shrinkage are also important and there is not only a need to improve and optimize these properties but also the possibility of devising materials showing novel thermal, electrical, magnetic or optical behaviour.

The physical properties, other than mechanical, have been discussed in a number of reviews [1–7] but most of these have been concerned primarily with the properties of directionally solidified eutectics, or with non-structural applications rather than basic properties. This review is concerned essentially with the relationships between the physical behaviour of composite materials and their structure. Discussion of the mechanical properties is excluded except where some consideration of the mechanical properties is necessary for the discussion of properties such as thermal expansion or swelling and shrinkage.

For the purpose of this review it will be assumed that a composite material is a heterogeneous mixture of two or more homogeneous phases with at least one continuous solid phase or an interconnected mixture of solid phases such that the geometry is fixed and the material can be considered as a solid. The dimensions of a phase are assumed to be greater than about 10 nm (100 Å). On a macroscopic scale, that is on a scale which is large compared with the pore or particle diameter or with the periodicity of the structure, the material then behaves as a quasi-homogeneous solid with its own characteristic properties. The essential problem that has to be considered is that of how the properties of the composite depend on the properties of the separate phases, their volume fractions, dimensions and geometry. To simplify the discussion it will usually be assumed that there are only two phases and that voids are absent, or if they should be present, as in a foamed material, then the voids can be regarded as one of the two phases.

The selection of a suitable plan for the discussion of the physical properties of composites presents some difficulties. The scheme adopted in this review is similar in many ways to that used by Albers [1] in discussing the physical properties of *in situ* composites. Two broad headings have been used to divide the physical properties into:

(1) properties determined by the properties of the constituent phases, their volume fractions and the composite geometry, and

(2) properties depending on structural factors such as periodicity and particle or fibre dimensions.

These two groups of properties are considered in turn. In Section 2 we examine the way in which the value, say A^*, of a given property depends on the fixed values A_1, A_2 ... for the component phases. The properties considered in Section 3 depend primarily on structural factors such as periodicity, inter-fibre spacing, particle dimensions etc (cf. the importance of the inter-particle distance on the mechanical properties of dispersion-strengthened metals). The properties considered include the optical, magnetic and superconducting properties; heat transfer under conditions where phase dimensions are important is also discussed. In Section 4 we consider the special case of "product properties" to which attention has been drawn by van Suchtelen [8] and Albers [1]. The discussion of some special properties including those associated with the Hall effect and resulting from a combination of different properties forms the subject of the final section.

The aim of this review has not been a comprehensive account of the physical properties but rather a discussion of representative properties with some indication of the ways in which "materials engineering" can be used to design and construct composite materials with predetermined properties using the theoretical and experimental information that is at present available.

2. Properties determined by the properties of the constituent phases, their volume fractions and the composite geometry

2.1. General considerations

Many of the physical properties of materials are described by a functional relation between a solenoidal vector and an irrotational vector: for example, for a linear isotropic material we have the relations

$$\mathbf{D} = \epsilon \mathbf{E} \tag{1}$$

where $\mathbf{D}$ is the electric induction, ϵ the dielectric constant and $\mathbf{E}$ the electric field and

$$\mathbf{B} = \mu \mathbf{H} \tag{2}$$

where $\mathbf{B}$ is the magnetic induction, μ the magnetic permeability and $\mathbf{H}$ the magnetizing force.

The coefficient of thermal conductivity is defined by Fourier's law which for an isotropic medium may be written in the form

$$\mathbf{J} = -\lambda \operatorname{grad} T \tag{3}$$

where λ, the thermal conductivity, is the proportionality constant between the heat flux vector $\mathbf{J}$ and the temperature gradient. Other transport coefficients are defined in a similar way as proportionality constants between fluxes and gradients. Examples are the electrical conductivity (Ohm's law) and diffusion coefficients (Fick's law).

With a composite material, the relations derived for all these properties will be formally identical and the expressions obtained for the dielectic constant, for example, will be equally applicable to the thermal conductivity or magnetic permeability.

In this section, we therefore first consider the dielectric constant of a composite and then the mathematically related properties such as the electrical and thermal conductivities. Next we consider the thermal expansion together with the swelling and shrinkage behaviour. Properties associated with time-dependent vector fields, in particular dielectric loss, fall outside the scope of this review.

To simplify the discussion, it will be assumed that the composite consists of two phases only, although in some cases general relationships for a property of an N-phase composite may have been derived. It is also assumed that both phases are isotropic. We have to remember, however, that even if the phases are isotropic in a particular property, the composite may be anisotropic in structure so that, with the composite, the property may be different in different directions.

It is assumed that the composite is statistically homogeneous, i.e. if we take small elements of the material then these will all have the same physical properties as the whole sample provided that the elements are large enough compared with the periodicity or dimensions of the phase regions to ensure that they are representative. Within an element, however, the geometry may be regular or irregular, isotropic or anisotropic. We may, for example, have a random dispersion of spherical particles in a continuous matrix, a regular array of aligned filaments, continuous laminae, or a completely irregular geometry with continuous or discontinuous phase regions (Fig. 1).

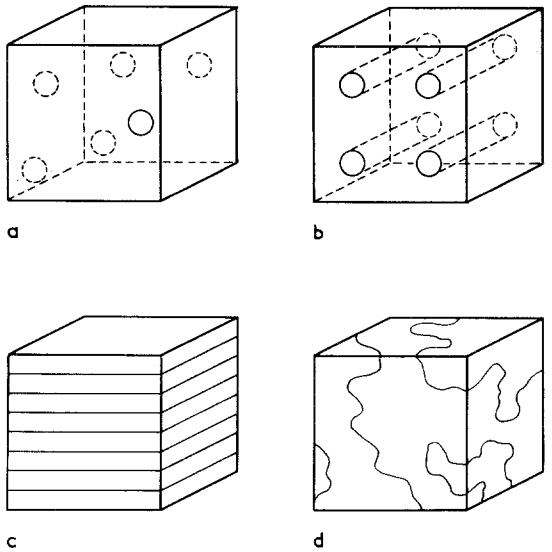

Figure 1 Composite geometries: (a) random dispersion of spheres in a continuous matrix, (b) regular array of aligned filaments, (c) continuous laminae, (d) irregular geometry.

The physical behaviour of a composite can be predicted with an exactitude which depends on the precision with which the phase geometry can be specified. In a fundamentally important paper [9], Brown showed that the dielectric constant of a composite must depend not only on the dielectric constants of the two phases and their volume fractions but also on the composite geometry. Attempts to derive *exact* theoretical expressions of general applicability for the dielectric constants of mixtures of unknown phase geometry are futile.

The dielectric constant ϵ^* of a mixture of two phases must, however, lie between certain limits whatever the geometry, and if some knowledge of the phase geometry is available, still closer bounds can be set on the possible value of ϵ^*. The same is true of other properties. For a few special geometries exact solutions can be obtained. Approximate solutions have also been obtained for two-phase composites with various geometries but these are, in general, only applicable when the volume fraction of one of the components is low.

2.2. Dielectric constants

The earlier theoretical work on the dielectric behaviour of heterogeneous systems has been described in some detail in the critical review by Van Beek [10]. The following summary includes some of the more important relationships derived in this earlier work together with results obtained in more recent theoretical investigations. The dielectric constant of the composite is represented by ϵ^*, the upper and lower bounds by $\epsilon^*_{(+)}$ and $\epsilon^*_{(-)}$, and the volume fractions of the two phases by V_1 and V_2. We first consider the effective dielectric constants of isotropic composites and then, in view of their technological importance for other properties, the relations for the dielectric constants of fibre composites.

2.2.1. Isotropic composites

Exact relations are available for very dilute dispersions of particles in a continuous matrix. Some of the more important expressions for the dielectric constants of suspensions containing a small volume fraction (V_1) of randomly oriented particles (dielectric constant ϵ_1) in a continuous matrix (dielectric constant ϵ_2) are included in Table I. Equation 4 is the Rayleigh mixture formula which was first derived for a cubical array of spheres. If $V_1(\epsilon_1 - \epsilon_2)/(2\epsilon_2 + \epsilon_1) \ll 1$ it may be written in the

TABLE I Formulae for the dielectric constants of isotropic two-phase composites containing randomly orientated particles in a continuous matrix

System	Dilute suspension $\epsilon_m = \epsilon_2$	References	SCS approximation $\epsilon_m = \epsilon^*$	References
Spheres	$\epsilon^* = \epsilon_2 \dfrac{2\epsilon_2 + \epsilon_1 + 2V_1(\epsilon_1 - \epsilon_2)}{2\epsilon_2 + \epsilon_1 - V_1(\epsilon_1 - \epsilon_2)}$ (4)	[11]		
	$\epsilon^* = \epsilon_2 + \dfrac{3V_1\epsilon_2(\epsilon_1 - \epsilon_2)}{2\epsilon_2 + \epsilon_1}$ (5)	[10]	$\epsilon^* = \epsilon_2 + \dfrac{3V_1\epsilon^*(\epsilon_1 - \epsilon_2)}{2\epsilon^* + \epsilon_1}$ (9)	[13]
Discs or lamellae	$\epsilon^* = \epsilon_2 + \dfrac{V_1(\epsilon_1 - \epsilon_2)(\epsilon_2 + 2\epsilon_1)}{3\epsilon_1}$ (6)	[12]	$\epsilon^* = \epsilon_2 + \dfrac{V_1(\epsilon_1 - \epsilon_2)(\epsilon^* + 2\epsilon_1)}{3\epsilon_1}$ (10)	[12]
Rods, needles or fibres	$\epsilon^* = \epsilon_2 + \dfrac{V_1(\epsilon_1 - \epsilon_2)(5\epsilon_2 + \epsilon_1)}{3(\epsilon_1 + \epsilon_2)}$ (7)	[10]	$\epsilon^* = \epsilon_2 + \dfrac{V_1(\epsilon_1 - \epsilon_2)(5\epsilon^* + \epsilon_1)}{3(\epsilon^* + \epsilon_1)}$ (11)	[10, 14]

simpler form given by Equation 5. This relation, together with Equations 6 and 7 for dilute suspensions of discs and rods, may be obtained from the general expression derived by Polder and Van Santen [15] for the dielectric constant of a dilute suspension of ellipsoids with a random distribution of orientations

$$\epsilon^* = \epsilon_2 + \frac{V_1(\epsilon_1 - \epsilon_2)}{3} \sum_{abc} \frac{\epsilon_m}{[\epsilon_m + A_i(\epsilon_1 - \epsilon_m)]} \tag{8}$$

where ϵ_m is the effective mean value of the dielectric constant of the medium around each particle and the A_i are the depolarizing factors along the ellipsoid axes a, b and c. Values for depolarizing factors have been tabulated by Stoner [16]; for spheres the depolarizing factors are $A_i = \frac{1}{3}$.

For very dilute suspensions, ϵ_m is equal to ϵ_2 the dielectric constant of the matrix. At higher concentrations, the disturbing effects of neighbouring particles on the field have to be considered. One way of doing this is to use the self-consistent scheme (SCS) in which it is assumed that each particle is surrounded by the composite material with a dielectric constant ϵ^* rather than by matrix with a dielectric constant ϵ_2. Setting ϵ_m equal to ϵ^* in Equation 8 then leads to Equations 9, 10 and 11 in Table I. Equation 9 which was derived by Böttcher [13] can be shown to be symmetrical in V_1 and V_2 $(= 1 - V_1)$ and it can be argued that it is an appropriate approximation for a conglomerate of particles of two different materials.

The assumption that each particle is surrounded by a continuum with a dielectric constant ϵ^* is, however, clearly an over-simplification. A more satisfactory assumption with a concentrated suspension of spherical particles might be to suppose that each particle (radius a) is surrounded by a shell of matrix (outer radius b) and that this, in turn, is surrounded by composite material. The extension of the SCS approach in this way has been discussed by Hashin [17] in a critical assessment of the SCS approximation. A special situation arises when

$$\frac{a^3}{b^3} = \frac{V_1}{V_2} \tag{12}$$

since it is then possible to construct a system in which the space within the material is completely filled by spheres of varying diameter each surrounded by its own shell of matrix with a thickness appropriate to the volume fraction. With this structural geometry which Hashin terms the composite spheres assemblage, the dielectric constant of the composite is given *exactly* by

$$\epsilon^* = \epsilon_2 + \frac{V_1}{[1/(\epsilon_1 - \epsilon_2)] + (V_2/3\epsilon_2)}. \tag{13}$$

For the corresponding case in which material 2 is the particulate phase and material 1 is the matrix, the dielectric constant of the composite is given by

$$\epsilon^* = \epsilon_1 + \frac{V_2}{[1/(\epsilon_2 - \epsilon_1)] + (V_1/3\epsilon_1)}. \tag{14}$$

It may be noted that Equations 13 and 14 are mathematically equivalent to the corresponding Rayleigh mixture formulae given by Equation 4.

Although real composite materials may have a structure approximating to the composite sphere assemblage, there will be uncertainty about the degree of approximation involved in using Equations 13 or 14, The same is true of the SCS approximations and the other approximate relations which have been derived for the dielectric constants of isotropic composites.

Rigorous upper and lower bounds can, however, be set on the value for the dielectric constant of a composite material and the use of these bounds may clearly be preferable to the use of uncertain approximations. The earliest bounds for the dielectric constant of a two-phase isotropic composite were those obtained by Wiener [18] and given by Equations 15 and 16 in Table II. These bounds have also been obtained by Brown using two minimization theories of classical electrostatics [19] and, since the expressions are identical with those for the longitudinal and transverse dielectric constants of a composite with alternating laminae, they are also the best possible bounds in the absence of any information on the geometry or degree of isotropy. The form of these bounds for $\epsilon_1/\epsilon_2 = 0.1$ and 0.01 is shown in Fig. 2.

Closer bounds for the effective dielectric constant of an isotropic composite were derived by Hashin and Shtrikman [20] using variational principles and are given by Equations 17 and 18 in

TABLE II Bounds for the dielectric constants of isotropic two-phase composites

Wiener [18]

$$\epsilon^*_{(+)} = \epsilon_1 V_1 + \epsilon_2 V_2 \tag{15}$$

$$\epsilon^*_{(-)} = \frac{1}{(V_1/\epsilon_1) + (V_2/\epsilon_2)} \tag{16}$$

Hashin and Shtrikman [20]

$$\epsilon^*_{(+)} = \epsilon_2 + \frac{V_1}{[1/(\epsilon_1 - \epsilon_2)] + (V_2/3\epsilon_2)} \tag{17}$$

$$\epsilon^*_{(-)} = \epsilon_1 + \frac{V_2}{[1/(\epsilon_2 - \epsilon_1)] + (V_1/3\epsilon_1)} \tag{18}$$

where $\epsilon_2 > \epsilon_1$

Beran [22]

$$\epsilon^*_{(+)} = \left[\langle\epsilon\rangle - \frac{\langle(\epsilon')^2\rangle}{3\langle\epsilon\rangle + (9\langle\epsilon\rangle^2/\langle(\epsilon')^2\rangle)I}\right] \tag{19}$$

$$\epsilon^*_{(-)} = \left[\left\langle\frac{1}{\epsilon}\right\rangle - \frac{(4/9\langle\epsilon\rangle^2)\langle\epsilon'/\epsilon\rangle^2}{(1/3\langle\epsilon\rangle^2)\langle(\epsilon')^2/\epsilon\rangle + J}\right]^{-1} \tag{20}$$

where

$$I = \frac{1}{16\pi^2\langle\epsilon\rangle^2}\int_{V_s}\int_{V_r}\left(\frac{\delta^2\langle\epsilon'(0)\epsilon'(r)\epsilon'(s)\rangle}{\delta r_3\,\delta s_3}\right)\frac{r_i s_i}{r^3 s^3}\,drds$$

$$J = \frac{1}{16\pi^2\langle\epsilon\rangle^2}\int_{V_s}\int_{V_r}\left(\frac{\delta^2\langle\epsilon'(r)\epsilon'(s)/\epsilon(0)\rangle}{\delta r_3\,\delta s_3}\right)\frac{r_i s_i}{r^3 s^3}\,drds$$

$\epsilon(x)$ = dielectric constant at point x

$\epsilon'(x) = \epsilon(x) - \langle\epsilon\rangle$

$\langle\epsilon\rangle$ = ensemble average of $\epsilon(x)$ (assumed to be equal to the spatial average)

$\langle\epsilon'(0)\epsilon'(r)\epsilon'(s)\rangle$ = ensemble average of the product of ϵ' at some co-ordinate origin within the composite, ϵ at a position r from the origin and ϵ' at position s.

r, s = sets of three orthogonal space vectors with a common origin.

V_r, V_s = volumes of infinite spheres in vector spaces denoted by subscripts.

Table II. The Hashin and Shtrikman bounds always lie within the Wiener bounds and, since they correspond exactly with Equations 13 and 14 for the two composite sphere assemblages, they are the best possible bounds for the dielectric constant of an isotropic two-phase material if no structural information apart from the volume fractions is available. If the values of ϵ_1 and ϵ_2 do not differ greatly the bounds are close together, but when the ratio of ϵ_2 to ϵ_1 is high the bounds become widely separated as shown in Fig. 2 in which the Hashin and Shtrikman bounds are compared with the Wiener bounds and the SCS approximation given by Equation 9 for a suspension of spherical particles. The dielectric constants of all isotropic composites containing dispersed spheres in a continuous matrix should, of course, fall within the Hashin and Shtrikman bounds and if the values of ϵ_1 and ϵ_2 do not differ greatly these bounds can show good agreement with experimental results. A good example is shown in Fig. 3 in which the Hashin and Shtrikman bounds are compared with Reynolds' experimental results [10, 21] for a suspension of glass spheres in carbon tetrachloride.

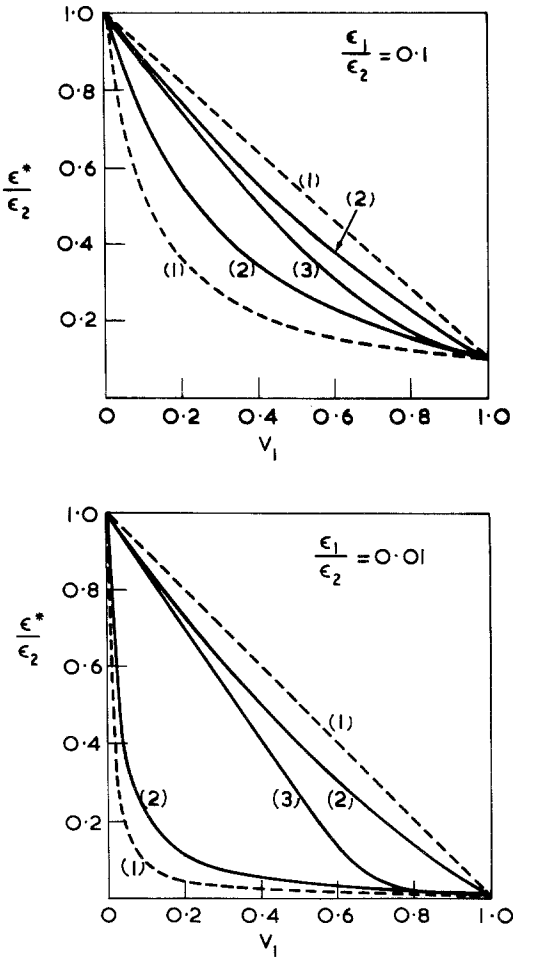

Figure 2 Dielectric constant of composite materials ($\epsilon_1/\epsilon_2 = 0.1$ and $\epsilon_1/\epsilon_2 = 0.01$). (1) Wiener bounds (equations 15 and 16), (2) Hashin and Shtrikman bounds for arbitrary geometry (Equations 17 and 18), (3) Böttcher SCS approximation for spheres in a continuous matrix (Equation 9).

If some information on the structural geometry is available, then closer bounds may be set of the value of the dielectric constant for an isotropic

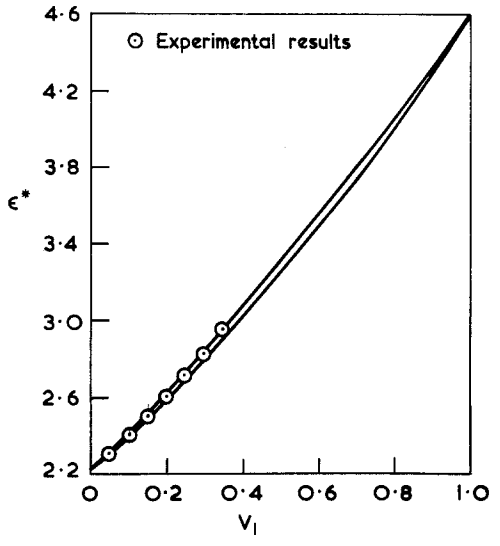

Figure 3 Dielectric constant of composite materials: Hashin and Shtrikman bounds and experimental results for glass spheres in carbon tetrachloride [10,21].

composite. To do this, statistical information is needed in addition to a knowledge of the volume fraction. Mathematically, this information can be introduced through n-point correlation functions which are related to the probability that n points thrown at random into the composite will all be in the same phase. Following the earlier work by Brown [9], Beran [22] obtained bounds for the dielectric constant using a variational principle which included the three-point correlation function. These bounds are given by Equations 19 and 20 in Table II. The application of statistical continuum theories of this kind to the prediction of the properties of heterogeneous materials has recently been examined by Corson [23–26]. For the experimental determination of a correlation function, the associated probability functions have to be measured. The technique developed by Corson involved preparing sections of the material, taking random photomicrographs, superimposing a matrix of points on each of the photomicrographs as a sampling grid, and then noting in which phase each point fell. From the experimental observations, the two- and three-point probability functions can be obtained and these can then be used to form the two- and three-point correlation functions. (The procedure used by Corson for deriving these correlation functions is complex and the original papers should be consulted for details.) Using the correlation functions, Corson evaluated the Beran bounds and then compared these with experimental data obtained with porous sandstone and firebrick (Fig. 8). The Beran bounds showed a significant improvement over the Hashin and Shtrikman bounds but the comparison with experimental results cannot be considered rigorous since it was assumed that the phase geometries of the porous sandstone and firebrick were similar to that of the iron–lead composites used in the experimental measurement of the spatial correlation functions.

As we have seen, the derivation of the Beran bounds presents serious problems. Miller [27], however, showed that for a broad class of isotropic two-phase composites which he termed cell materials, the problem could be circumvented. For these materials, he deduced that the functions of the three-point correlation function which appeared in the bounds for ϵ^* were simply a number for each material with a value between $\frac{1}{9}$ and $\frac{1}{3}$ with the number having a simple geometric significance (e.g. $\frac{1}{9}$ for a spherical cell). Miller obtained bounds for two types of material–symmetrical and asymmetrical cell materials.

In the symmetrical cell materials the space within the composite is subdivided by closed surfaces into closed regions or cells so that the following requirements are met:

(1) the space is completely filled by cells;

(2) the cells are distributed in such a way that the material is statistically homogeneous and isotropic;

(3) the dielectric constant ϵ of a particular cell is statistically independent of the dielectric constant in any other cell;

(4) the conditional probabilities of n points being and m points not being in the same cell of a particular material, given that one point is in a cell of that material, are the same for each material.

Miller gives three examples of symmetrical cell materials. The first example is the Poisson cell material in which the space within the composite is divided into convex polyhedron-shaped cells. In the second example, the cells no longer have plane or convex sides but are star-shaped instead. The third example is a composite built up of spheres with diameters varying in such a way that the space within the composite is completely filled.

With the asymmetrical cell materials the geometry of the cells of the two materials is dissimilar. In this case, the space within the composite is subdivided so that the following requirements are fulfilled:

(1) the space is completely filled by cells;

TABLE III Miller's bounds for the dielectric constants of isotropic two-phase cell materials [27]

$$\epsilon^*_{(+)} = \epsilon_2\left[1 + \phi(\alpha-1) - \frac{\frac{1}{3}\phi(1-\phi)(\alpha-1)^2}{1+(\alpha-1)\{\phi + 3[(1-\phi)^2 G_1 - \phi^2 G_2]\}}\right] \quad (21)$$

$$\epsilon^*_{(-)} = \epsilon_1\left[[\alpha - \phi(\alpha-1)] - \frac{\frac{4}{3}\phi(1-\phi)(\alpha-1)^2}{1+\alpha+3(\alpha-1)[\phi^2 G_2 - (1-\phi)^2 G_1]}\right]^{-1} \quad (22)$$

where $\phi = V_1$, $1-\phi = V_2$, $\alpha = \epsilon_1/\epsilon_2$ and G_1 and G_2 are shape factors for the two materials ($\frac{1}{9}$ for spheres, $\frac{1}{3}$ for discs, and $\frac{1}{6}$ for needles).
For asymmetrical cell materials $G_1 \neq G_2$
For symmetrical cell materials $G_1 = G_2 = G$

(2) the cells are distributed in such a way that the material is statistically homogeneous and isotropic;

(3) the dielectric constant ϵ of a particular cell is statistically independent of the dielectric constant in any other cell.

An example of an asymmetrical cell material is a composite formed from spheres and cubes of varying size. It is assumed that the space within the material can be completely filled without any preference as to whether a cube or sphere is inserted in any given location.

For these two-phase cell materials, Miller obtained the bounds given by Equations 21 and 22 in Table III. The shape factors G_1 and G_2 are simple numbers each lying between $\frac{1}{9}$ and $\frac{1}{3}$, and characteristic of the cell geometries of the two materials. If G_1 is equal to G_2 then these equations represent the bounds for the symmetrical cell materials. The bounds shown in Table III have also been derived by McCoy [28].

The extreme upper bound is given by Equation 21 with $G_1 = \frac{1}{3}$ and $G_2 = \frac{1}{9}$; the extreme lower bound by Equation 22 with $G_1 = \frac{1}{9}$ and $G_2 = \frac{1}{3}$. For all possible values of α, ϕ, G_1 and G_2, these bounds for the asymmetrical cell materials fall inside the Hashin and Shtrikman bounds. This is, at first sight, unexpected since the Hashin and Shtrikman bounds actually correspond to the relations for a real physical geometry (the composite spheres assemblage discussed above). This particular geometry cannot, however, be represented by the asymmetrical cell model.

When ϕ approaches zero or unity, and α also approaches unity, the bounds for the symmetrical cell material ($G_1 = G_2 = G$) converge and become coincident with the exact solution for the dielectric constant of a suspension containing particles of a corresponding shape at very low concentration. The appropriate values for G which should be used in these bounding equations can, therefore, be found by letting ϕ approach zero or unity and α approach unity and then setting the solution equal to the small concentration solution to solve for G. If an exact small concentration solution is not available (e.g. with particles of irregular shape) a G value may be obtained from experimental measurements on a suspension at low concentrations.

This cell model would seem to be intrinsically suitable for the representation of the behaviour of materials with a cell-like structure such as eutectic alloys or sintered materials. The appropriate G values will then be determined by the geometries of the component cells. The Miller bounds can also, as described below, be applied to systems in which particles are dispersed in a continuous matrix, i.e. suspensions. With, for example, a suspension of spheres, the space between the spheres which is filled with matrix material is assumed to be made up of cells of all shapes and sizes so that the fundamental requirements of the asymmetrical cell model are satisfied. The bounds are then obtained by the following method. At low concentrations of material 1, i.e. when ϕ is small, the bounds given by Equations 21 and 22 can be written in the form

$$\frac{\epsilon^*_{(+)}}{\epsilon_2} = 1 + \phi(\alpha-1)\left\{1 - \frac{\alpha-1}{3[1+3(\alpha-1)G_1]}\right\} \quad (23)$$

and

$$\frac{\epsilon^*_{(-)}}{\epsilon_2} = 1 + \phi\frac{(\alpha-1)}{\alpha}\left\{1 + \frac{4(\alpha-1)}{3[1+\alpha-3(\alpha-1)G_1]}\right\}. \quad (24)$$

If $\epsilon^*_{(+)}$ is set equal to $\epsilon^*_{(-)}$, a quadratic equation in G_1 is obtained with the roots $G_1 = \frac{1}{3}$ and $G_1 = \frac{1}{9}$. If G_1 is set equal to $\frac{1}{9}$ then Equations 23 and 24 become equivalent to

Equation 5, the solution for a dilute suspension of spheres, so that Miller concludes that $G_1 = \frac{1}{9}$ has the geometrical significance of a sphere.

The bounds for a suspension of spheres when the spheres have the higher dielectric constant, are then obtained from Equations 21 and 22 by setting $G_1 = \frac{1}{9}$ and G_2 equal to a value in the range $\frac{1}{9}$ to $\frac{1}{3}$ which gives the highest upper and the lowest lower bound. If the spheres have the lower dielectric constant then G_2 is set equal to $\frac{1}{9}$. The Miller bounds for the dielectric constant of a suspension of spheres in a continuous matrix ($\epsilon_1/\epsilon_2 = 10$) are shown in Fig. 4 together with the corresponding Hashin and Shtrikman bounds and the Rayleigh mixture formula.

For a suspension of randomly oriented discs, we can set G_1 in Equations 23 and 24 equal to $\frac{1}{3}$ and then these equations become equivalent to Equation 6 so that $G_1 = \frac{1}{3}$ has the geometrical significance of a disc. The bounds are then obtained from Equations 21 and 22 by setting $G_1 = \frac{1}{3}$ and G_2 to a value in the range $\frac{1}{9}$ to $\frac{1}{3}$ which gives the highest upper and the lowest lower bound.

Similarly, closer bounds on the dielectric constant of a composite containing randomly oriented needles can be set when the geometry

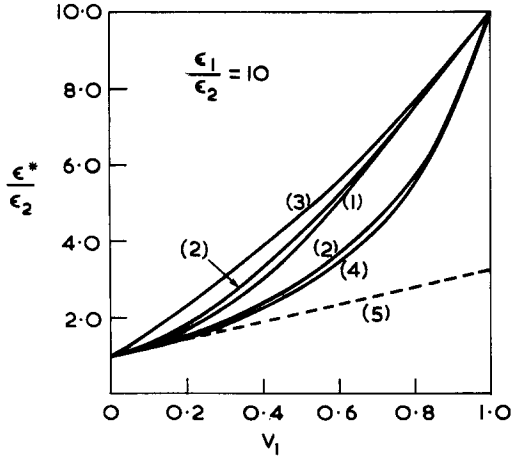

Figure 4 Equations for the dielectric constant of a suspension of spheres in a continuous matrix ($\epsilon_1/\epsilon_2 = 10$). (1) Böttcher's SCS approximation (Equation 9). (2) Upper and lower bounds for Miller asymmetric cell model (Equations 21 and 22). (3) Upper Hashin and Shtrikman bound (Equation 17); composite spheres assemblage with spheres of material 2 in material 1 (Equation 14). (4) Lower Hashin and Shtrikman bound (Equation 18); composite spheres assemblage with spheres of material 1 in material 2 (Equation 13); Rayleigh mixture formula (Equation 4). (5) Rayleigh mixture formula for very dilute solutions (Equation 5).

meets the requirements of Miller's asymmetrical cell model. A G value of $\frac{1}{8}$ is obtained for needles [27] by solving Equations 23, 24 and 7 for small perturbations (i.e. α approaches unity).

The bounds for particle suspensions obtained using Miller's model are substantially closer than the Hashin and Shtrikman bounds for volume fractions up to about 0.6. In practice, however, there may be some doubt as to when a system can be represented by the asymmetrical cell model. The composite spheres assemblage in particular cannot be represented in this way since the dielectric constants for systems of this type lie outside the Miller bounds.

2.2.2. Aligned rods, needles, or fibres

If the rods or fibres are of uniform cross-section and aligned in one direction then the dielectric constant of the composite in the axial direction (ϵ_A^*) is given by

$$\epsilon_A^* = V_1\epsilon_1 + V_2\epsilon_2. \tag{25}$$

This result is independent of the transverse geometry.

For a dilute suspension of fibres with a circular cross-section, the transverse dielectric constant is given by Rayleigh's formula for cylinders [10, 11]

$$\frac{\epsilon_T^* - \epsilon_2}{\epsilon_T^* + \epsilon_2} = V_1\frac{\epsilon_1 - \epsilon_2}{\epsilon_1 + \epsilon_2} \tag{26}$$

Using a self consistent scheme in which $\bar{\epsilon} = \epsilon^*$, Davies [14] obtained the expression

$$\epsilon_T^* = \epsilon_2 + \frac{2V_1\epsilon_T^*(\epsilon_1 - \epsilon_2)}{\epsilon_T^* + \epsilon_1} \tag{27}$$

which corresponds with that given by Peterson and Hermans [29] for aligned cylinders perpendicular to the field. Numerical solutions have also been given by Springer and Tsai [30].

For a composite cylinder assemblage similar to the composite sphere assemblage described above, Hashin [5] showed that

$$\epsilon_T^* = \epsilon_2 + \frac{V_1}{[1/(\epsilon_1 - \epsilon_2)] + (V_2/2\epsilon_2)}. \tag{28}$$

This relationship is mathematically identical to Equation 26.

Hashin also showed that the bounds for the transverse dielectric constant of a transversely

isotropic fibre reinforced material were given by

$$\epsilon^*_{T(+)} = \epsilon_2 + \frac{V_1}{[1/(\epsilon_1 - \epsilon_2)] + (V_2/2\epsilon_2)}, \tag{29}$$

and

$$\epsilon^*_{T(-)} = \epsilon_1 + \frac{V_2}{[1/(\epsilon_2 - \epsilon_1)] + (V_1/2\epsilon_1)}. \tag{30}$$

Since Equation 29 is identical to Equation 28 and Equation 30 with the result for a composite cylinder assemblage in which material 2 is the fibre and material 1 the matrix, it follows that Equations 29 and 30 are the best possible bounds for the transverse dielectric constant of a transversely isotropic fibre composite if the only information available is the volume fractions and the dielectric constants of the two phases.

When additional geometrical information is available, closer bounds can be set on the transverse dielectric constant. Thus, using a composite cylinder model similar to that used by Hashin and Rosen [31] for mechanical properties, Donea [32] derived bounds for the transverse thermal conductivity of a composite containing aligned fibres of identical circular cross-section arranged in a square or hexagonal array.

Bounds for the transverse dielectric constant of an aligned fibre composite with additional information on the fibre geometry have also been obtained by Beran and Silnutzer [33] using a method of analysis closely similar to that followed by Beran and Miller [22, 27] in deriving bounds for the isotropic three-dimensional composite. It was, in fact, only necessary to rewrite all the previous results using two rather than three dimensions. This then gave the following equations for the upper and lower bounds

$$\frac{\epsilon^*_{(+)}}{(\epsilon_1\epsilon_2)^{1/2}} = \frac{1}{\alpha^{1/2}}\left[1 + V_1(\alpha - 1) - \frac{\frac{1}{2}V_1V_2(\alpha-1)^2}{1 + (\alpha-1)(V_1 + 2V_2^2G_1 - 2V_1^2G_2)}\right], \tag{31}$$

and

$$\frac{\epsilon^*_{(-)}}{(\epsilon_1\epsilon_2)^{1/2}} = \alpha^{1/2}\Bigg/\left\{V_1 + V_2\alpha - \left[\frac{\frac{1}{4}(1-\alpha)^2V_1V_2}{(\alpha-1)(V_1^2G_2 - V_2^2G_1) + (\alpha/2) + (1-\alpha/2)V_1}\right]\right\} \tag{32}$$

where, as before, $\alpha = \epsilon_1/\epsilon_2 > 1$. G_1 and G_2 are two numbers lying within the range $\frac{1}{4}$ to $\frac{1}{2}$ which characterize the fibre and matrix geometries. A G value of $\frac{1}{4}$ corresponds to a circular shape and $G = \frac{1}{2}$ to the shape of parallel lamellae (two-dimensional needles). These bounds always lie between the Hashin bounds. Beran and Silnutzer consider the fibre geometry to be of first importance since at low concentrations the term $V_2^2G_1$ will be much larger than $V_1^2G_2$.

For circular fibres, the bounds are quite close up to volume fractions of about 0.2 when $\alpha = 10$ and up to about 0.1 when $\alpha = 100$. In both cases the bounds are close to the Hashin lower bound. When the volume fractions are of the order of 0.50, however, the bounds diverge considerably. Beran and Silnutzer concluded that the packing geometry is extremely important and that changing the positioning of the fibres would have a significant effect on the value of ϵ^*_T.

This analysis has been taken a stage further by Elsayed and McCoy [34] who have derived bounds which incorporate additional geometrical information in the form of further shape factors and two packing parameters.

2.2.3. Fibres randomly oriented in a plane

For fibres randomly oriented in a plane, Davies [14] obtained the SCS-type relations

$$\epsilon_z = \epsilon_2 + \frac{2V_1\epsilon_z(\epsilon_1 - \epsilon_2)}{\epsilon_z + \epsilon_1} \tag{33}$$

$$\epsilon_x = \epsilon_y = \epsilon_2 + \frac{V_1(\epsilon_1 - \epsilon_2)(\epsilon_1 + 3\epsilon_x)}{2(\epsilon_x + \epsilon_1)}. \tag{34}$$

2.2.4. Conducting inclusions

For a composite system containing dispersed conducting particles ϵ_1 is very much greater than ϵ_2 and approximate equations for the dielectric constant can then be derived for $\epsilon_1 \to \infty$. For example, for spherical particles, when $\epsilon_1 \gg \epsilon_2$ and $\bar{\epsilon} = \epsilon_2$ we have the relation

$$\epsilon^* = \epsilon_2(1 + 3V_1) \tag{35}$$

instead of Equation 5. For insulators (e.g. air cavities) in a matrix with a high dielectric constant $\epsilon_1 \ll \epsilon_2$ and for spherical inclusions we then have,

$$\epsilon^* = \epsilon_2(1 - \tfrac{3}{2}V_1). \tag{36}$$

The derivation of these and similar relations has been discussed by van Beek [10].

2.3. Electrical conductivity

All the expressions given in the previous section are also valid for the electrical conductance of a two-phase composite. It is only necessary to replace ϵ_1, ϵ_2, ϵ^*, $\epsilon^*_{(+)}$, $\epsilon^*_{(-)}$ etc by the conductances σ_1, σ_2, σ^*, $\sigma^*_{(+)}$, $\sigma^*_{(-)}$ etc. Many of the expressions derived specifically for the resistance or conductance of a composite are indeed mathematically identical with corresponding expressions for the dielectric constant. For example, Maxwell's equation [35] for the specific resistance of a dilute suspension of spheres is

$$\rho^* = \frac{2\rho_1 + \rho_2 + V_1(\rho_1 - \rho_2)}{2\rho_1 + \rho_2 - 2V_1(\rho_1 - \rho_2)}\rho_2. \quad (37)$$

When the specific resistances are replaced by the corresponding conductances, this becomes mathematically identical with the Rayleigh mixture formula for dielectrics (Equation 4). Similarly, the expression for the electrical conductivity of a two-phase composite derived by Landauer [36] using a self-consistent scheme approximation,

$$V_1 \frac{\sigma_1 - \sigma^*}{\sigma_1 + 2\sigma^*} + V_2 \frac{\sigma_2 - \sigma^*}{\sigma_2 + 2\sigma^*} = 0 \quad (38)$$

corresponds with Equation 9 derived by Böttcher for the dielectric system.

In applying the expressions given in Section 2.2 to experimental results, it must however be remembered that they involve the implicit assumption that interface effects such as space charge polarization are absent, i.e. it is necessary to assume that the potentials on opposite sides of the interface but infinitely near to each other are equal and that the current through any element of the surface is the same when measured in either medium [35]. With two solid phases, deviations from the theory may be expected if voids are present, but voids in a single solid phase can be regarded as a separate non-conducting phase.

Landauer examined the application of Equation 38 to experimental data on the electrical resistance of binary metallic mixtures. In seven cases (Bi–Bi_2Pb, Bi–Sn, Cd–Pb, Cu–Fe, Cu_2Sb–Sb, Mg_2Pb–Pb, Pb–Sb) where agreement with a mixture theory might be expected, five gave good agreement. A comparison of the experimental values for the Cu_2Sb–Sb system and the theoretical curve is shown in Fig. 5. With the Mg_2Pb–Pb system, however, the results failed to

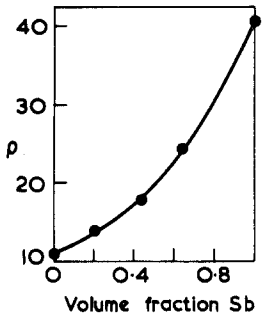

Figure 5 Comparison of experimental values for the resistivity of the Cu_2Sb–Sb system [167] with theoretical curve obtained from Equation 38 (after Landauer [36]).

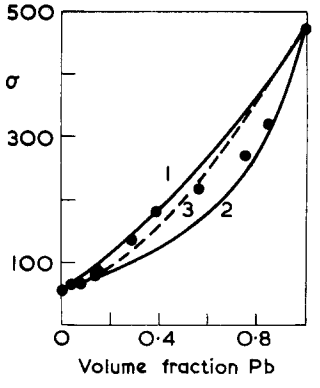

Figure 6 Comparison of experimental values for conductivity of the Mg_2Pb–Pb system [168] with theory. (1) Equation 17. (2) Equation 18. (3) Equation 38. (After Hashin [5]).

fit the theory. The experimental values in this case do, however, fall inside the Hashin and Shtrikman bounds which, in this case, are not too far apart (Fig. 6).

In the extreme case of composites containing conducting particles in an insulating matrix, the dominant factor determining the conductivity at the higher particle volume fractions would appear to be the formation of infinite chains of particles in contact with one another [37–40]. At the lower volume fractions these chains are unlikely to be formed and the conductivity of the composite does not differ greatly from that of the matrix. The relationships between the number of particle contacts and the degree of continuity have been discussed by Gurland [41].

2.4. Thermal conductivity

As we have noted earlier, the relations given for the dielectric constant in Section 2.2 will also

apply to steady-state heat conduction and can be used to derive the effective thermal conductivities of two-phase composite materials. Many of the relations given in Section 2.2 have indeed been rederived or reapplied in the analysis of thermal conduction. The formula given by Brailsford and Major [42]

$$\frac{\lambda^*}{\lambda_2} = \left[1 - 2V_1\left(\frac{1-\lambda_1/\lambda_2}{2+\lambda_1/\lambda_2}\right)\right] \Bigg/ \left[1 + V_1\left(\frac{1-\lambda_1/\lambda_2}{2+\lambda_1/\lambda_2}\right)\right] \quad (39)$$

for the thermal conductivity of a two-phase aggregate in which particles of phase 1 (thermal conductivity λ_1 and volume fraction V_1) are surrounded by a continuous phase 2 (thermal conductivity λ_2) corresponds to Equation 4 for the dielectric constant and to Equation 37 for the specific resistance. These equations should however only be applicable to dilute suspensions. For systems in which no special circumstances lead to the spatial continuity of either phase and each phase can be treated equivalently, Brailsford and Major [42] suggested the possible application of an SCS type equation corresponding to Equation 38 derived by Landauer for the electrical conductivity. A large number of empirical or semi-empirical expressions for the thermal conductivity of heterogeneous systems have also been examined. As with the dielectric constant it will, however, only be possible to obtain a satisfactory description of the thermal conductivity behaviour by taking the geometry of the composite into consideration and making proper use of the geometrical information that is available.

Problems of heat transfer are of considerable technological importance in situations where heat transfer has to be encouraged, as in heat exchangers, or reduced by the use of insulation. Most insulating materials are, indeed, essentially mixtures of a solid material and air and owe their insulating properties to the low thermal conductivity of air which, in the absence of convection and under dry conditions, has a value of 2.45×10^{-2} W m^{-1} K^{-1} at 273° K. (The air may, of course, in some cases be replaced by another gas or a vacuum.) The insulating material can have a fibrous or granular structure (e.g. glass wool or diatomaceous earth) in which case the air is the continuous phase or it can be cellular (e.g. a polyurethane foam). In the latter case, if the pores are open there will be two continuous phases; if they are closed there will be one continuous solid phase.

For a foamed or porous material, the thermal conductivity λ is often expressed as

$$\lambda = \lambda_s + \lambda_g + \lambda_r + \lambda_c \quad (40)$$

where λ_s, λ_g, λ_r and λ_c are contributions due to conduction through the solid, conduction through the gas, radiation and convection within the pores. This description is, however, misleading since it implies that the four processes are taking place independently and in parallel. At normal temperatures, however, radiation effects will be small and, if the cell diameter is less than 3 to 4 mm, convection effects will be negligible [43]. For isotropic materials with small pores, cavities or interstices it can then be assumed that the thermal conductivity is determined by the thermal conductivities of the phases and the phase geometry. Use can then be made of the Hashin and Shtrikman bounds given by Equations 17 and 18. These bounds for the air/silica system are shown in Fig. 7 in which the thermal conductivities of various insulating materials have been plotted against their densities. The thermal conductivity of silica (1.36 W m^{-1} K^{-1}) does not differ very greatly from that of gypsum (1.30 W m^{-1} K^{-1}) and the values for diatomaceous earth, rock wool, powdered gypsum and cellular gypsum all fall within the Hashin and Shtrikman bounds. It can be seen immediately from Fig. 7 that it will be impossible to make an isotropic composite from air and silica with a thermal conductivity of less than 0.05 W m^{-1} K^{-1} unless the density of the composite is less than 625 kg m^{-3}. It may also be noted that the values for cellular gypsum in which the solid phase is continuous lie towards the upper bound while those for powdered gypsum lie towards the lower bound.

With this type of system in which there is a large difference between the thermal conductivities of the two components, the Hashin and Shtrikman bounds are very widely separated and more geometrical information is clearly needed to predict the thermal conductivity of the composite material. In Fig. 8 the Beran bounds calculated by Corson [26] are compared with the experimental values obtained by Sugawara and Yoshizawa [45] for the effective thermal conductivity of firebrick. The Beran bounds are closer than the Hashin and

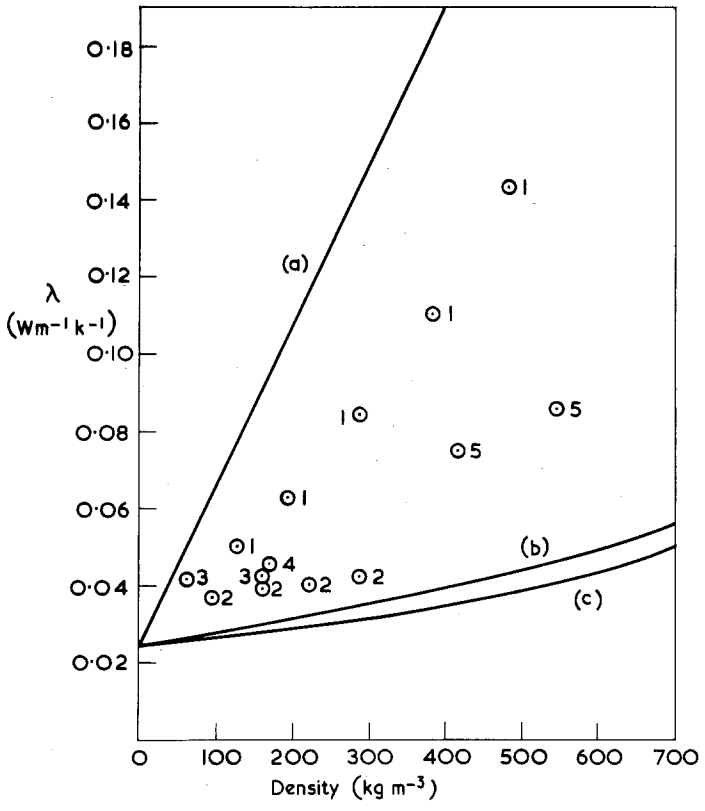

Figure 7 Thermal conductivity of insulating materials. Theoretical curves: (a) Hashin and Shtrikman upper bound for air-silica, (b) Hashin and Shtrikman lower bound, (c) Davies relation for fibres randomly oriented in a plane. Experimental results: (1) cellular gypsum, (2) rock wool, (3) glass wool, (4) diatomaceous earth, (5) powdered gypsum (data from [169]).

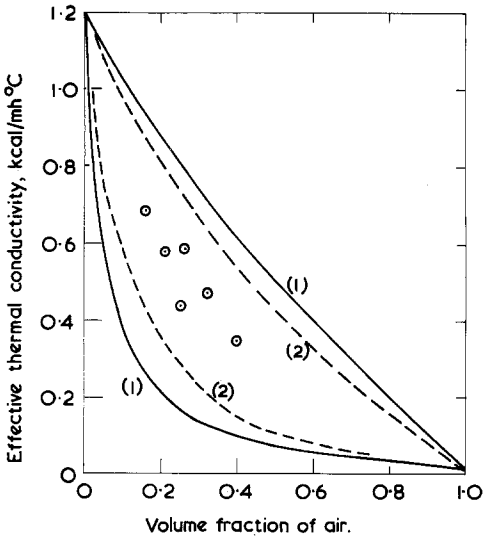

Figure 8 Effective thermal conductivity of fire-brick (after Corson [26]). (1) Hashin and Shtrikman bounds, (2) Beran bounds. (Experimental data from Sugawara and Yoshizawa [45]).

Shtrikman bounds but are still, however, widely separated.

Fibrous insulating materials will usually be anisotropic but more or less isotropic in a plane. With glass-fibre insulation under normal conditions

TABLE IV Thermal conductivity of fibrous insulating materials

Conduction through air	0.027 W m^{-1} K^{-1}
Convection	0.003 W m^{-1} K^{-1}
Radiation	0.002 W m^{-1} K^{-1}
Conduction through solid	0.002 W m^{-1} K^{-1}
Total conductivity	0.034 W m^{-1} K^{-1}

the thermal conductivity is largely determined by the conductivity of the enclosed air, but radiation and convection can make significant contributions especially when compared with that due to conduction through the solid. Table IV [44] gives details of the contributions due to the different mechanisms if it is assumed that these operate independently and in parallel.

If we neglect convection and radiation effects, the thermal conductivity of a composite containing fibres randomly oriented in a plane can be estimated using Equation 33. A theoretical curve calculated from this equation assuming that, for the fibres, $\lambda = 1.0$ W m^{-1} K^{-1} and $\rho = 2600$ kg m^{-3}, has been included in Fig. 7. It will be seen that the experimental results for the rock wool and glass wool insulation follow the same general trend but the experimental values are appreciably higher. This is presumably the result of the effects

of radiation, convection, fibre–fibre contacts, or out-of-plane fibre alignment.

In the absence of effects due to radiation and convection, the thermal conductivity of a composite is, under normal conditions, independent of the particle size [46] or inter-fibre spacing provided these are (a) sufficiently small for the material to be considered macroscopically homogeneous and (b) sufficiently large compared with the mean free path of the carrier (e.g. electrons or phonons) responsible for the conduction process. The use of the relations given in Section 2.2 does, however, involve the assumption that there is no discontinuity or barrier at the interface which, in the presence of a heat flux, would lead to the temperature on one side of the interface being different from that on the other. With particle-filled materials, e.g. filled elastomers, voids may be expected to lead to anomalous behaviour [47].

The conditions under which phase dimensions can become important in heat transfer are considered in Section 3.4.

2.5. Thermal expansion coefficients

Thermal expansion behaviour can be important when composite materials are used in conjunction with other materials and when it is necessary to match the thermal expansion coefficient of one structural component with another. An important function of reinforcing fillers and fibres in plastics is the reduction and control of the thermal expansion. With dental filling materials a difference in thermal expansion between the filling material and the tooth substance can lead to a marginal gap (Fig. 9). With the composite filling materials which have a thermal expansion coefficient very much closer to that of tooth substance these effects are very much reduced [48].

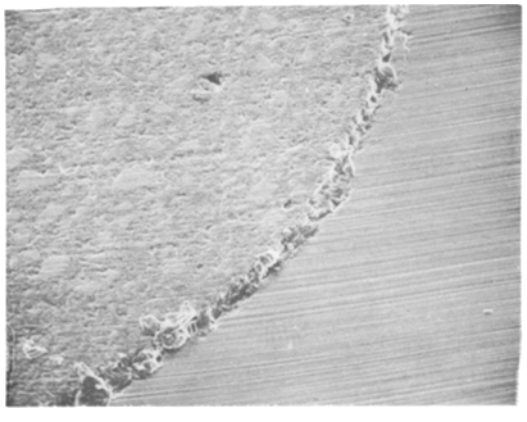

Figure 9 Scanning electron micrograph (× 100) showing marginal gap produced by difference in thermal expansion coefficients of dental filling material and tooth substance (courtesy Dr W. Finger).

The effective thermal expansion coefficients for a composite material are defined as the average strains which result from unit temperature rise in a traction-free material. In considering the response of composite materials to changes in temperature, the basic stress-strain relations which are used in defining the elastic moduli have to be modified to include the thermal expansion coefficient. Levin [49], in an important paper, showed that a simple relationship between the effective expansion coefficients and the effective elastic moduli could be derived for two-phase materials using the thermoelastic stress–strain relations. For an isotropic composite with two isotropic phases the basic relationship can be written in the form

$$\alpha^* = \bar{\alpha} + \frac{\alpha_1 - \alpha_2}{[(1/K_1) - (1/K_2)]}\left[\frac{1}{K^*} - \overline{\left(\frac{1}{K}\right)}\right] \tag{41}$$

where α_1, α_2 are the linear thermal expansion coefficients of the two phases, K_1, K_2 are their bulk moduli, K^* and α^* the effective bulk modulus and effective thermal expansion coefficient of the composite, and the bars over the symbols indicate volume averages [50]. The relationship represented by Equation 41 has also been established by Schapery [51], Cribb [52] and Steel [53].

The form of Equation 41 gives an indication of how the effective expansion coefficient will deviate from the simple mixture rule, $\alpha^* = \bar{\alpha}$, as a result of the mechanical interactions represented by the final term. If one of the phases is a fluid (or a low shear modulus matrix) and the other consists of rigid particles

$$\frac{1}{K^*} \simeq \overline{\left(\frac{1}{K}\right)} \tag{42}$$

and it follows from Equation 41 that $\alpha^* \simeq \bar{\alpha}$, and the mixture rule will apply [51].

It also follows from Equation 41 that if we know the values of K_1 and K_2 and can calculate K^*, then we can also calculate α^* from α_1 and α_2 for any given volume fraction V_1. If we cannot calculate K^* but can set bounds on its value then we can also set bounds on the value of α^*.

The simplest case for a statistically isotropic material is that of a dilute suspension of spherical

particles when we can make use of the relation derived by Hashin [54].

$$K^* = K_2 + (K_1 - K_2)\frac{3K_2 + 4\mu_2}{3K_1 + 4\mu_1} V_1 \tag{43}$$

for a dilute suspension in which spherical particles with bulk modulus K_1 are dispersed in a matrix with bulk modulus K_2 and shear modulus μ_2. This relation may be expected to apply when the volume fraction of the particles V_1 does not exceed a few per cent. From Equation 41 and 43 we obtain

$$\alpha^* = \alpha_2 + \frac{(\alpha_1 - \alpha_2)K_1(3K_2 + 4\mu_2)V_1}{K_2(3K_1 + 4\mu_2) + (K_1 - K_2)(3K_2 + 4\mu_2)V_1} \tag{44}$$

or, neglecting the final term in the denominator of the last term

$$\alpha^* = \alpha_2 + \frac{(\alpha_1 - \alpha_2)K_1(3K_2 + 4\mu_2)V_1}{K_2(3K_1 + 4\mu_2)} . \tag{45}$$

For higher particle concentrations, the composite sphere assemblage described in Section 2.2.1 may be a more realistic model since it incorporates an element of randomness and its use involves the implicit assumption that each composite sphere is, in effect, surrounded by composite material instead of matrix. For the effective bulk modulus of this system, Hashin [24] obtained the exact relation

$$K^* = K_2 + (K_1 - K_2)\frac{(3K_2 + 4\mu_2)V_1}{3K_1 + 4\mu_2 + 3(K_2 - K_1)V_1} . \tag{46}$$

When V_1 is small, the last term in the denominator of the final term can be neglected and the relation then becomes identical with Equation 43. An expression corresponding to Equation 46 for the effective bulk modulus was obtained earlier by Kerner [55] but the method of derivation is difficult to understand [5].

If we substitute Equation 46 in Levin's equation Equation 41 we obtain the relation

$$\alpha^* = \alpha_2 - \frac{(\alpha_2 - \alpha_1)K_1(3K_2 + 4\mu_2)V_1}{K_2(3K_1 + 4\mu_2) + 4(K_1 - K_2)\mu_2 V_1} \tag{47}$$

for the effective linear thermal expansion coefficient of the composite sphere assemblage. This relation can also be obtained from the expressions given by Kerner [55]. It may be noted that when $V_1 = 0$, $\alpha^* = \alpha_2$, when $V_1 = 1$, $\alpha^* = \alpha_1$ and when $\mu_2 = 0$, $\alpha^* = \alpha_1 V_1 + \alpha_2 V_2$.

Using the relationships

$$K = \frac{E}{3(1 - 2\nu)} \quad \text{and} \quad \mu = \frac{E}{2(1 + \nu)} \tag{48}$$

where E is Young's modulus and ν is Poisson's ratio, Equation 47 can be written in the form

$$\alpha^* = \alpha_2 - (\alpha_2 - \alpha_1)V_1 \times \frac{3(E_1/E_2)(1 - \nu_2)}{(E_1/E_2)[2V_1(1 - 2\nu_2) + (1 + \nu_2)] + 2(1 - 2\nu_1)V_2} \tag{49}$$

which corresponds with the relations obtained by Wang and Kwei [56] and Fahmy and Ragai [57] from a consideration of the displacements and stresses in a composite sphere.

When the composite consists of a mixture of two kinds of particle, rather than particles of one phase dispersed in a continuous matrix, the SCS approximation described in Section 2.2.1 may be more appropriate since, in this case, each phase is considered on an equal footing. The effective thermal expansion coefficient α^* will be given by Equation 41 with K^* determined by the relations

$$K^* = K_2 + (K_1 - K_2)\frac{3K^* + 4\mu^*}{3K_1 + 4\mu^*} V_1 \tag{50}$$

$$\mu^* = \mu_2 + (\mu_1 - \mu_2) \times \frac{5(3K^* + 4\mu^*)V_1}{9K^* + 8\mu^* + 6(K^* + 2\mu^*)(\mu_1/\mu^*)} \tag{51}$$

These two expressions which were derived independently by Budiansky [58, 59] and Hill [60] will, in general, have to be solved numerically to obtain K^*, but decouple when $\nu_1 = \nu_2 = 0.2$ [59]. Similar expressions, which reduce to Equations 50 and 51, were also given by Kerner [55]. The use of the self-consistent

method for determining thermoelastic moduli has also been discussed by Laws [61].

If the geometry of the composite is not clearly defined it can be argued that it is better to use rigorous bounds rather than an uncertain approximation. Bounds on the effective thermal expansion coefficient of an isotropic composite can be obtained by using Paul's bounds [62] on the bulk modulus:

$$\frac{1}{\bar{K}} \leqslant \frac{1}{K^*} \leqslant \overline{\left(\frac{1}{K}\right)}. \tag{52}$$

As we have seen, the lower bound on K^* represented by Equation 42 and corresponding to uniform stress in the composite leads to the "mixture rule", $\alpha^* = \bar{\alpha}$, when substituted into Equation 41. The upper bound on K^* corresponding to uniform strain and given by

$$K^* = K_1 V_1 + K_2 V_2 \tag{53}$$

leads with Equation 41 to the relation

$$\alpha^* = \frac{K_1 \alpha_1 V_1 + K_2 \alpha_2 V_2}{K_1 V_1 + K_2 V_2} = \frac{\overline{K\alpha}}{\bar{K}}, \tag{54}$$

which is the expression suggested by Turner [63] for the thermal expansion coefficient of a two-phase composite.

Closer bounds on the value of α^* can, however, be set by using the bounds derived by Hashin and Shtrikman [64], Hill [65] and Walpole [66] for the bulk modulus, which may be written in the form

$$K^*_{(-)} = K_1 + \frac{V_2}{[1/(K_2 - K_1)] + [3V_1/(3K_1 + 4\mu_1)]} \tag{55a}$$

$$K^*_{(+)} = K_2 + \frac{V_1}{[1/(K_1 - K_2)] + [3V_2/(3K_2 + 4\mu_2)]} \tag{55b}$$

where $\mu_2 > \mu_1$. When $\mu_1 > \mu_2$, the relations for the upper and lower bounds are reversed and when $\mu_1 = \mu_2$, the bounds coincide.

These bounds and the Levin relationship (Equation 41) lead to the following bounds for α^*:

$$\alpha^*_{(-)} = \alpha_1 - \frac{(\alpha_1 - \alpha_2)K_2(3K_1 + 4\mu_1)V_2}{K_1(3K_2 + 4\mu_1) + 4(K_2 - K_1)\mu_1 V_2} \tag{56}$$

$$\alpha^*_{(+)} = \alpha_2 - \frac{(\alpha_2 - \alpha_1)K_1(3K_2 + 4\mu_2)V_1}{K_2(3K_1 + 4\mu_2) + 4(K_1 - K_2)\mu_2 V_1}, \tag{57}$$

where

$$\frac{\alpha_2 - \alpha_1}{K_2 - K_1} > 0 \quad \text{and} \quad \mu_2 > \mu_1.$$

When $(\alpha_2 - \alpha_1)/(K_2 - K_1) < 0$ or $\mu_2 < \mu_1$, the bounds are reversed. When $\alpha_2 = \alpha_1$ or $\mu_2 = \mu_1$, the bounds coincide.

It should be noted that Equation 57 for the upper bound $\alpha^*_{(+)}$ is identical with Equation 47 for the effective thermal expansion coefficient of the composite sphere assemblage in which spheres of material 1 are surrounded by shells of material 2. Similarly, Equation 56 will correspond to the relation for the effective thermal expansion coefficient of a composite sphere assemblage in which spheres of material 2 are surrounded by shells of material 1. This means that, as with the bounds for bulk modulus [5], the bounds given by Equations 56 and 57 are the best possible bounds for the effective thermal expansion coefficient of an isotropic composite of arbitrary geometry.

If, however, further statistical information on the composite geometry is available closer bounds can be set than those given by the Hashin and Shtrikman results. Thus, bounds for the bulk modulus have been derived by Beran and Molyneux [67] and McCoy [68] using the information contained in the three-point correlation function. These bounds are, unfortunately, complex expressions involving derivatives and integrals of the correlation functions and, in their original form, cannot be easily used except in special cases. Miller [69], however, showed that bounds on the bulk modulus of the two-phase cell materials described in Section 2.2.1 could be obtained in the form of relatively simple algebraic functions from the Beran and Molyneux expressions. These bounds depend on the values of K_1, K_2, μ_1, μ_2, V_1 and V_2 and on the two parameters G_1 and G_2 which describe the cell

TABLE V Axial and transverse thermal expansion coefficients for transversely isotropic aligned fibre composites

Levin [49]

$$\alpha_a^* = \alpha_2 + \frac{(\alpha_1 - \alpha_2)}{(\nu_1 - \nu_2)E_a^*}[(1+\nu_1)(E_a^* - V_2E_2) - (1+\nu_2)V_1E_1] \quad (60)$$

$$\alpha_t^* = \alpha_2 + \frac{(\alpha_1 - \alpha_2)}{(\nu_1 - \nu_2)E_a^*}[(1+\nu_1)(V_2\nu_a^*E_2 - \nu_2E_a^*) + V_1\nu_a^*E_1(1+\nu_2)] \quad (61)$$

Schapery [51]

$$\alpha_a^*\frac{E_a^*}{\bar{E}} - \frac{\overline{E\alpha}}{\bar{E}} = \frac{\alpha_1(1+\nu_1) - \alpha_2(1+\nu_2)}{\nu_1 - \nu_2}\left(\frac{E_a^* - E}{\bar{E}}\right) \quad (62)$$

Rosen [70]

$$\alpha_a^* = \bar{\alpha} + \left[\frac{\alpha_1 - \alpha_2}{(1/K_1) - (1/K_2)}\right]\left[\frac{3(1-2\nu_a^*)}{E_a^*} - \overline{\left(\frac{1}{K}\right)}\right] \quad (63)$$

$$\alpha_t^* = \bar{\alpha} + \left[\frac{\alpha_1 - \alpha_2}{(1/K_1) - (1/K_2)}\right]\left[\frac{3}{2k_t^*} - \frac{3\nu_a^*(1-2\nu_a^*)}{E_a^*} - \overline{\left(\frac{1}{K}\right)}\right] \quad (64)$$

Van Fo Fy [71]

$$\alpha_t^* = \alpha_2 + (\alpha_2 - \alpha_a^*)\nu_a^* - (\alpha_2 - \alpha_1)(1+\nu_1)\frac{(\nu_2 - \nu_a^*)}{(\nu_2 - \nu_1)} \quad (65)$$

where the symbols have the following significance
α_a^*, α_t^* effective axial and transverse linear thermal expansion coefficients.
α_1, α_2 linear thermal expansion coefficients of fibre and matrix.
ν_1, ν_2 Poisson's ratio for fibre and matrix.
E_a^*, ν_a^* Young's modulus and Poisson's ratio of composite under axial loading.
E_1, E_2 Young's moduli for fibre and matrix.
K_1, K_2 bulk moduli for fibre and matrix.
k_t^* transverse plane-strain bulk modulus of composite and bars over symbols indicate volume averages, e.g.

$$\overline{E\alpha} = E_1\alpha_1V_1 + E_2\alpha_2V_2 \quad \text{and} \quad \overline{\left(\frac{1}{K}\right)} = \frac{V_1}{K_1} + \frac{V_2}{K_2}$$

geometries of the two materials. Miller showed that the values of G_1 and G_2 must lie between $\frac{1}{9}$ and $\frac{1}{3}$ and that, as for the dielectric case (see Section 2.2.1), a value of $\frac{1}{9}$ corresponded to a spherical shape and a value of $\frac{1}{3}$ to a plate-like shape.

The bounds for the asymmetrical cell material take the following form (after correcting some typographical errors in the equations given in Miller's paper),

$$\frac{K_{(+)}^*}{(K_1K_2)^{1/2}} = \frac{1}{\alpha^{1/2}}\left[1 + \phi(\alpha-1) - \left(\frac{\phi(1-\phi)(\alpha-1)^2}{\alpha - (\alpha-1)\phi + 2\gamma\{1 - \frac{4}{3}\phi + \frac{1}{3}\beta(4\phi-1) + 3(\beta-1)[G_1(1-\phi)^2 - G_2\phi^2]\}}\right)\right] \quad (58)$$

where $\alpha = K_1/K_2$, $\beta = \mu_1/\mu_2$, $\phi = V_1$, $\gamma = \mu_2/K_2$. The bounding equations for the symmetrical cell material can be obtained by setting $G_1 = G_2$ in Equations 58 and 59.

Up to now, it has been assumed that both the composite and the two constituent phases are isotropic. The more general case of multiphase anisotropic composites with anisotropic phases has been considered by Rosen and Hashin [50] who derived bounds both for the effective thermal

$$\frac{K_{(-)}^*}{(K_1K_2)^{1/2}} = \alpha^{1/2}\left\{\phi(1-\alpha) + \alpha - \left(\frac{\phi(1-\phi)(\alpha-1)^2}{1 + \phi(\alpha-1) + \frac{3}{8}(\alpha/\beta\gamma)[3(\beta-1)\{3[G_2\phi^2 - G_1(1-\phi)^2] - \frac{4}{3}\phi\} + 3\beta - 1]}\right)\right\}^{-1} \quad (59)$$

expansion coefficients and specific heats. In the case of two-phase composites the bounds coincide and give unique relations between the effective expansion coefficients and the effective elastic moduli. Rosen and Hashin also showed that these relationships for the two phase composite could be derived directly using the methods developed by Levin which they extended to include anisotropic phases.

In the important case of a transversely isotropic aligned fibre composite with two isotropic phases, a number of expressions have been derived for the axial and transverse thermal expansion coefficients. These are given in Table V. By making use of the relationships between the elastic moduli given by Equation 48, Hill's relations between the fibre composite moduli [72], and with some effort on the algebra, it can be shown that (a) the Levin, Schapery and Rosen expressions for the axial expansion coefficients are equivalent, (b) the Levin and Rosen equations for the transverse expansion coefficient are also equivalent, and (c) these expressions for the axial and transverse expansion coefficients then lead to the relationship given in Equation 65 between α_a^* and α_t^* previously given by Van Fo Fy [71].

From these relationships, bounds on the thermal expansion coefficients can be obtained from bounds on the moduli. For example, with Equations 60 to 62 in Table V, we can make use of the bounds derived by Hill [72] for the axial Young's modulus,

$$E^*_{a(+)} = E_1V_1 + E_2V_2 + \frac{4V_1V_2(\nu_1 - \nu_2)^2}{V_1/k_2 + V_2/k_1 + 1/\mu_1} \quad (66)$$

$$E^*_{a(-)} = E_1V_1 + E_2V_2 + \frac{4V_1V_2(\nu_1 - \nu_2)^2}{V_1/k_2 + V_2/k_1 + 1/\mu_2} \quad (67)$$

where k is the plane-strain bulk modulus given by

$$k = K + \tfrac{1}{3}\mu. \quad (68)$$

Alternatively, we can make use of the SCS method and either use the equations in Table V with the relations given by Hill [73] for the elastic moduli, or use the explicit formulae given by Laws [74] for the overall thermoelastic moduli.

Rosen [70] suggested the composite cylinder assemblage was an appropriate model and a similar approach has been adopted by Schneider [75, 76] who derived the following expressions for the thermal expansion coefficients using a model in which the fibres were aligned in a hexagonal array:

$$\alpha_a^* = \alpha_1 + \frac{\alpha_2 - \alpha_1}{(V_1/(1-V_1))\,E_1/E_2 + 1} \quad (68a)$$

$$\alpha_t^* = \alpha_2 - (\alpha_2 - \alpha_1) \times \left[\frac{2(\nu_2^2 - \nu_2 - 1)\,1.1\,V_1}{1.1\,V_1(2\nu_2^2 + \nu_2 - 1) - (1+\nu_2)} - \frac{\nu_2\,E_1/E_2}{E_1/E_2 + (1 - 1.1\,V_1)/1.1\,V_1}\right]. \quad (68b)$$

It may be noted that when $\nu_1 = \nu_2$, Equations 66 and 67 reduce to

$$E_a^* = E_1V_1 + E_2V_2. \quad (69)$$

On substituting this simpler relation for the axial Young's modulus in Equation 60 we obtain the simple approximate expression

$$\alpha_a^* = \frac{\alpha_1K_1V_1 + \alpha_2K_2V_2}{K_1V_1 + K_2V_2} \quad (70)$$

$$\alpha_a^* = \frac{\alpha_1E_1V_1 + \alpha_2E_2V_2}{E_1V_1 + E_2V_2}, \quad (71)$$

which in most cases will provide an adequate expression for the axial thermal expansion coefficient.

Some of the theoretical relationships described above are compared in Fig. 10 with the experimental results obtained by Schneider [75] for the axial and transverse thermal expansion coefficients of an aligned glass-fibre composite with an epoxy-resin matrix. The theoretical curves have been calculated using the following values for the properties of the glass fibre and epoxy-resin matrix. Glass: $E_1 = 71.59$ GN m^{-2}, $\nu_1 = 0.25$, $\alpha_1 = 4.8 \times 10^{-6}$ K^{-1}, $K_1 = 47.73$ GN m^{-2}, $\mu_1 = 28.64$ GN m^{-2}, $k_1 = 57.28$ GN m^{-2}. Epoxy-resin: $E_2 = 3.14$ GN m^{-2}, $\nu_1 = 0.4$, $\alpha_2 = 66 \times 10^{-6}$ K^{-1}, $K_2 = 5.23$ GN m^{-2}, $\mu_2 = 1.121$ GN m^{-2}, $k_2 = 5.60$ GN m^{-2}. The experimental results for α_a^* lie close to the lower bound obtained using Hill's relations for the bounds on the moduli (the theoretical curve corresponding to Equation 71 has not been plotted since it is extremely close

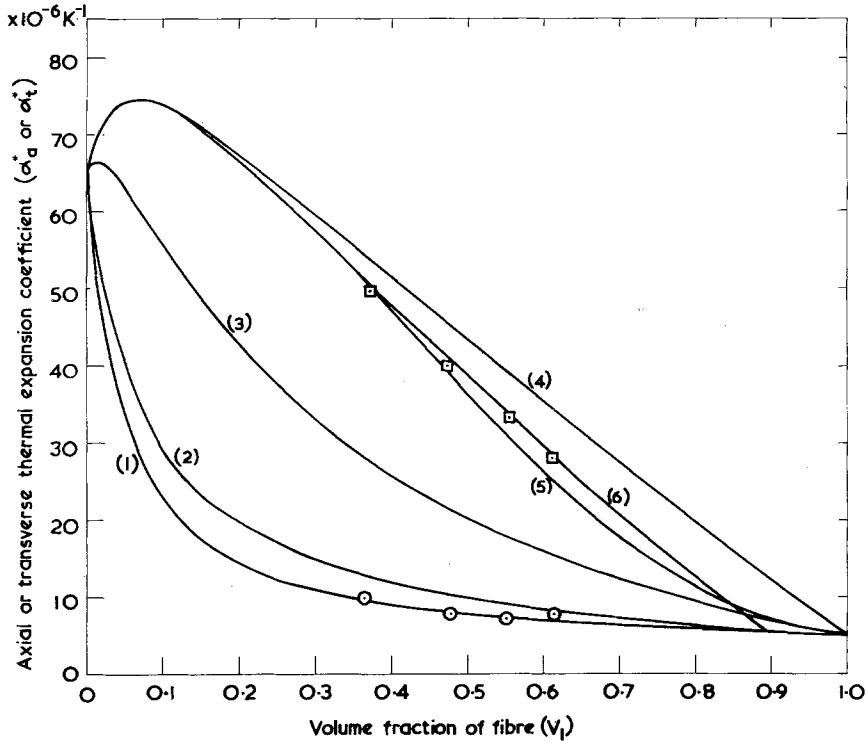

Figure 10 Thermal expansion of aligned glass-fibre composites. (1) Lower bound for α_a^*, (2) upper bound for α_a^*, (3) lower bound for α_t^*, (4) upper bound for α_t^*, calculated using Equations 60 and 61 with Hill's bounds on E_a^*. (5) SCS approximation for α_t^*, (6) Schneider's equation for α_t^*. Experimental results [75]: ⊙axial thermal expansion ⊡transverse thermal expension coefficient.

to this lower bound), The experimental values for α_t^* fall between the calculated bounds and lie close to the curves obtained using (a) the SCS approximation for the moduli and (b) Schneider's model.

From Fig. 10 it will be seen that, at low fibre volume fractions, the transverse expansion coefficient of the glass fibre–epoxy resin composite will be greater than that of the matrix. This effect will be especially noticeable with fibres of high modulus and low axial expansion coefficient (e.g. boron or carbon) in a low-modulus matrix (e.g. epoxy resin) [70].

The coefficient of linear thermal expansion of a unidirectional laminate at an angle to the fibre direction can be obtained from purely geometrical considerations [77]. At an angle θ, the expansion coefficient α_θ^* of a transversely isotropic laminate will be given by

$$\alpha_\theta^* = \alpha_t^* \sin^2\theta + \alpha_a^* \cos^2\theta. \quad (72)$$

Once the thermal expansion properties of a single layer of fibre-reinforced material have been derived, classical laminated plate theory [78–80] can be used to calculate the behaviour of a laminate in which the layers are of various orientations. In this theory each layer is treated as a homogeneous anisotropic material in a state of plane stress. The thermal expansion coefficient and the thermal stresses in multi-ply laminates have been considered in some detail by Schneider [76].

A balanced laminate in which the plies are oriented at angles of 0°, 60°, – 60° and 0° will show pseudoisotropic in-plane elastic behaviour and the thermal expansion within the plane will also be quasi-isotropic. Halpin and Pagano [81], however, showed that a laminate need not necessarily be quasi-isotropic with respect to in-plane stiffness for it to show isotropic in-plane thermal expansion behaviour. Isotropic thermal expansion within the plane will be shown by any uncoupled laminate with equal stiffnesses in two in-plane directions.

The effective in-plane thermal expansion coefficients α_1^* and α_2^* for "angle-ply" laminates in which the fibres are arranged at angles of $+\theta$ and $-\theta$ to the 1-direction have been evaluated both by Halpin and Pagano [81–83] and by Dow and

Rosen [84, 85]. With these angle-ply laminates a "scissoring" or "lazy tongs" type of action can occur and, with appropriate values of θ, lead to a zero or even a negative thermal expansion coefficient in one direction. Dow and Rosen found that a ratio of filament to matrix modulus of at least 25 to 50 was required to achieve pronounced "scissoring". Their theoretical analysis indicated that the boron/epoxy system would not quite give a zero thermal expansion in any of the 2–D configurations examined. However, a zero thermal expansion could be achieved theroretically with a 3–D configuration in which half the filaments in the comparable 2–D configuration were rotated about the 1-axis into a plane at 90° to the original plane. The general effects predicted both by Dow and Rosen and by Halpin and Pagano have been confirmed experimentally with carbon fibres in epoxy resin (86–89). With this system, negative coefficients of thermal expansion in one direction can be achieved. The thermal expansion of laminated fibre composites in the thickness direction has been investigated by Fahmy and Ragai-Ellozy [90].

Approximate values for the thermal expansion coefficients of oriented short fibre composites can be obtained [91] by estimating the stiffness in the fibre direction from that of the corresponding continuous fibre composite and assuming that Poisson's ratio for the matrix is the same as that for the fibre. Laminate theory can then be used to obtain the thermal expansion coefficient of randomly oriented short fibre laminates. If the aspect ratio is sufficiently high the properties of the randomly oriented discontinuous fibre composite can be predicted from the behaviour of a pseudo-isotropic laminate reinforced with continuous fibres [92].

Up to this point it has been assumed that the phases in the composite remain in contact at the interfaces and that, in particular, with two solid phases the composite remains fully bonded. The effects of internal stresses arising from differences in the expansion coefficients of the components have not been considered. These internal stresses can be important not only in the fabrication of the composite but also in determining its subsequent behaviour.

If we take the composite sphere assemblage as a model system, the interfacial pressure can be obtained by finding the pressure which has to be applied to the outside of the central sphere and the inside of the surrounding shell to compensate for the misfit due to differences in thermal expansion of the two materials. For a rise in temperature of ΔT the interfacial pressure P in an initially stress-free system is given by

$$P = -\frac{2(\alpha_2 - \alpha_1)\,\Delta T E_1 E_2}{2E_2 V_2(1-2\nu_1) + 2E_1 V_1(1-2\nu_2) + E_1(1+\nu_2)} \quad (73)$$

This relation corresponds with that given by Fahmy and Ragai [57] after correcting for an apparent error in sign in their published equation. When $V_1 \to 0$, the expression reduces to that obtained by Selsing [93] for a dilute suspension.

If $\alpha_2 > \alpha_1$ and ΔT is negative, then P will be positive and there will be a normal compressive stress at the interface. Thus if a particle-reinforced composite is fabricated at a temperature above ambient, a positive interfacial pressure will develop on cooling the composite to room temperature if the thermal expansion of the matrix is greater than that of the inclusions. On the other hand, if $\alpha_2 > \alpha_1$ and the temperature of an initially stress-free composite is raised, a normal tensile stress will develop at the interface. This may be sufficient to lead to debonding. If separation of the two components occurs at the interface then the expansion of the matrix will no longer be restrained by the inclusions and the thermal expansion of the composite will then be equal to that of the matrix [56, 94, 95]. With fibre-reinforced materials, the internal stresses resulting from changes in temperature may lead to multiple cracking of the matrix [96]. In considering the development of internal stresses during the fabrication of composites, other dilatational effects, e.g. the shrinkage of resins on cure, must also be taken into account. These effects are discussed in the following section.

2.6. Swelling and shrinkage

Volume changes in the solid components of a composite material may arise not only as a result of changes in temperature but also from other causes. Two of the more important are:

(a) a phase change or chemical reaction e.g. polymerization or cross-linking; and

(b) the absorption of gases, liquids or vapours.

The effects of phase changes or chemical reaction during fabrication are of importance with a wide range of composites: excessive shrinkage of

one component can result in high internal stresses which may lead to premature failure or even preclude successful fabrication. Matrix shrinkage also has important indirect effects on the mechanical behaviour of fibre composites since the consequent internal stresses can determine the frictional forces at the fibre–matrix interface. The problem of deducing the shrinkage of a composite in terms of the properties of its components is also of importance in the prediction of shrinkage in concrete [97, 98].

In principle, as indicated by Cribb [52], Equation 41 for the thermal expansion of a two phase composite can be expected to apply equally well to the prediction of strain arising from the shrinkage of one or both of the components as a result of phase changes or chemical reactions such as polymerization or the setting of cement. It will be merely necessary to replace the linear thermal expansion coefficients by the corresponding linear strains resulting from shrinkage. Indeed, relations of the type given in Section 2.5 should in general, be applicable not only for the prediction of the shrinkage of composites but also for the analysis of the resulting internal stresses. With processes such as resin polymerization or the setting of cement there is, however, a continuous change in the viscoelastic properties of the material and there will be some difficulty in deciding on appropriate values both for the linear shrinkage and the elastic moduli of the resin or the cement.

The importance of swelling behaviour was clearly recognized in early work [99] on cellulose fibre composites since with these systems both the fibre and resin matrix behaved as swelling gels which could absorb or desorb water depending on the environmental conditions. The consequent swelling and shrinkage of the composites could have serious adverse effects on their performance in structural situations. With composites based on glass, carbon or boron fibres, swelling and shrinkage arising through sorption or desorption of water does not have such a marked effect since although, with glass fibres in particular, water may be absorbed at the interface, these fibres are not swelling gels and do not absorb water in the same way as cellulose fibres. Swelling effects can, however, still be very important in the absorption of water by nylon composites and in the absorption of organic solvents by a wide range of reinforced polymers and elastomers.

Halpin and Pagano [81] considered that the deformation of a solid induced by swelling was equivalent to that caused by a temperature change and applied this concept to the analysis of the swelling behaviour of a unidirectionally reinforced composite sheet using Schapery's [51] formulae for linear thermal expansion coefficients. They showed that it was possible to predict the expansional strains of a nylon-reinforced elastomer in benzene within the limits of their experimental precision. They also showed that it should be possible to design laminates which would contract in one direction on swelling.

It would appear, however, that the Halpin and Pagano analysis involves the assumption that the weight of solvent absorbed by a given volume of polymer is not affected by fibre reinforcement and that the expansional strains in the composite are determined solely by the elastic deformations of the components. There would seem to be some doubt as to how far this assumption is justified at any rate with composites based on polymers to which the Flory–Rehner [100, 101] theory of swelling is applicable. On this interpretation the condition for the equilibrium swelling of a cross-linked polymer of the conventional type in which the ends of the chains are united tetrafunctionally is given by

$$\ln(1 - V_2) + V_2 + \mu V_2^2 + (\rho V_0/M_c)(V_2^{1/3} - V_2/2) = \frac{\mu_1 - \mu_0}{RT} \quad (74)$$

where V_2 is the volume fraction of unswollen polymer, μ is a dimensionless parameter characterizing the interaction energy of solvent and polymer, ρ is the density, V_0 is the molar volume, M_c is the number average molecular weight of the polymer chains between the cross-links, μ_1 the chemical potential of the solvent in the polymer and μ_0 the chemical potential of the pure solvent. For equilibrium with the pure solvent, $\mu_1 = \mu_0$ and the swelling of the unconstrained polymer will be given by

$$\ln(1 - V_2) + V_2 + \mu V_2^2 + (\rho V_0/M_c)(V_2^{1/3} - V_2/2) = 0. \quad (75)$$

If the polymer is under a hydrostatic pressure P, the swelling will be given by

$$\ln(1 - V_2) + V_2 + \mu V_2^2 + (\rho V_0/M_c)(V_2^{1/3} - V_2/2) = -\frac{PV_0}{RT} \quad (76)$$

when the correction term, $-V_2/2$ given by Flory [100] is included in Treloar's [101] equation. If swelling is constrained in one direction but can take place in the other two directions, we have [101, 102]

$$\ln(1 - V_2) + V_2 + \mu V_2^2 + (\rho V_0/M_c)(1 - V_2/2) = 0. \quad (77)$$

The application of this relationship to the swelling in toluene of unidirectionally reinforced rubber composites has been examined by Coran *et al.* [102]. Although the constraint due to the reinforcement reduced the amount of solvent absorbed, the swelling in a direction perpendicular to the reinforcement was actually higher than that in the unreinforced material. Good agreement was obtained between the experimental results and those predicted by Equation 77. The effect of mechanical constraints on the sorption of water by cell wall material in wood was examined by Barkas [103] who considered that an elastic sheath surrounding the cell wall material exerted a natural restraint on the swelling of the wood substance. The swelling of wood from the standpoint of composite theory, has also been considered by Cave [104].

As with thermal expansion, differential swelling of matrix and reinforcement in a composite can lead to debonding at the interface. Thus, for example, with polyester fibre composites, resin swelling in water at 100° C was sufficient to overcome the effects of resin shrinkage during cure, producing a net tensile stress across the fibre-resin interface with the result that both untreated carbon fibres and untreated glass fibres were rapidly debonded [105, 106]. At 20° C, untreated glass fibres were debonded but the interfacial bond was retained with both the carbon fibres and treated glass fibres.

3. Properties determined by phase dimensions and structural periodicity

In the preceding sections, the properties under consideration have been dependent on the volume fractions and geometries of the phases but not on the phase dimensions (provided these are small compared with the size of the specimen). The expressions given for the effective properties do not include any dimensional parameters so that, for example, the effective dielectric constant of a dilute suspension of spherical particles does not depend on the particle radius.

The dimensions and periodicity of a composite structure may, however, have an important effect on the properties when they become comparable with, for example, the wavelength of incident radiation, the size of magnetic domains or the thickness of space charge layers at interfaces. Interface effects will, in general, become more important as the dimensions are decreased.

The effects will be especially noticeable in composites in which the particle radius is less than some critical value and in composites with a periodic structure in which the spacing between aligned fibres or lamellae is fixed and defined. Composites with structures of the latter type can be prepared by the unidirectional solidification of eutectics or eutectoids. With eutectics, the interlamellar period λ is given by $\lambda^2 R =$ a constant where R is the imposed growth rate; for eutectoids, $\lambda^4 R =$ a constant [107]. Another possible method of preparation is by the unidirectional decomposition of non-crystalline solid single-phase materials [108].

Properties dependent on phase dimensions and periodicity include some of the optical, magnetic and superconducting properties. Under certain conditions, phase dimensions can also become important in heat transfer through composite materials.

3.1. Optical and related effects

Many of the optical effects which depend on structural dimensions also depend in a complex way on other factors, the theory can be extremely complicated, and a detailed discussion is beyond the scope of this review. The more important effects arise in light scattering and diffraction.

For very small particles with a size very much less than the wavelength λ of the incident light, the intensity of scattered light is given by the Rayleigh relationship which for unpolarized incident light and a single particle takes the form

$$I = \frac{I_0 8\pi^4 \alpha^2}{r^2 \lambda^4} (1 + \cos^2\theta), \quad (78)$$

where I is the intensity of the scattered light at a distance r from the particle, I_0 the intensity of the incident light, α the polarizability of the particle, λ the wavelength, and θ the angle between the scattered and incident light. The quantity $I_{90} r^2 / I_0 V$ where V is the volume of the particle is known as the Rayleigh ratio $R_{(90)}$.

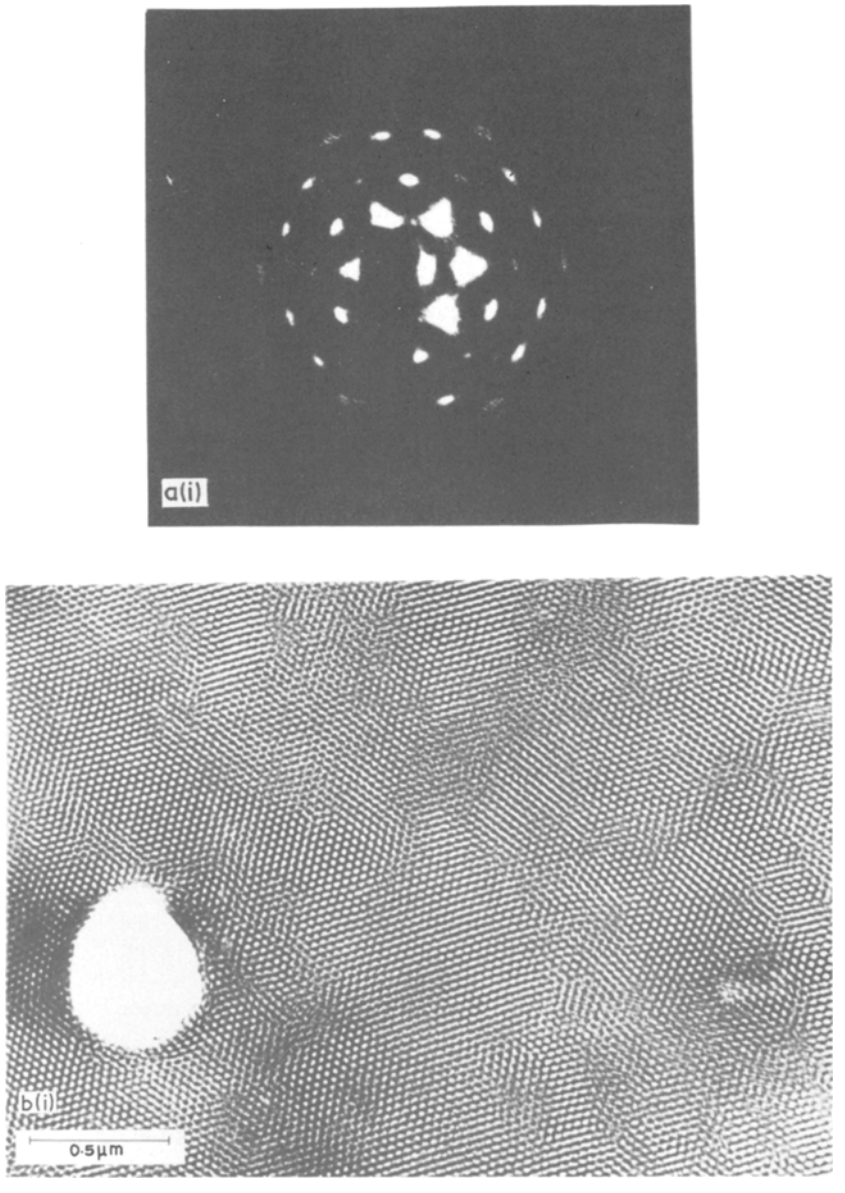

Figure 11 Extruded polystrene–polybutadiene–polystyrene block co-polymer (a) low-angle X-ray diffraction [118]: (i) beam parallel to extrusion direction; (ii) beam perpendicular; (b) electron micrographs [119] of sections cut (i) perpendicular and (ii) parallel to extrusion direction. 1.0. (Courtesy Professor A. Keller and Dr J. Dlugosz.)

For an assembly of particles we can assume, in the simplest approximation, that the particles are very far apart and the intensity of the light scattered by N particles will then be given by

$$I_N = \frac{N I_0}{r^2} \frac{8\pi^4 \alpha^2}{\lambda^4} (1 + \cos^2\theta). \qquad (79)$$

The polarizability α depends on the volume V of one particle so that α^2 will be proportional to V_2. With a given volume of particles, N will be inversely proportional to V. The light scattered by a given volume concentration of the particulate phase will, therefore, increase as the particle size increases. This general principle forms the basis for the determination of the molecular weights of high polymers (and simpler molecules) in solution by light-scattering measurements [109] using the theory developed by Debye [110, 111].

The effect of particle size on the light scattering behaviour in a solid medium is very well illustrated

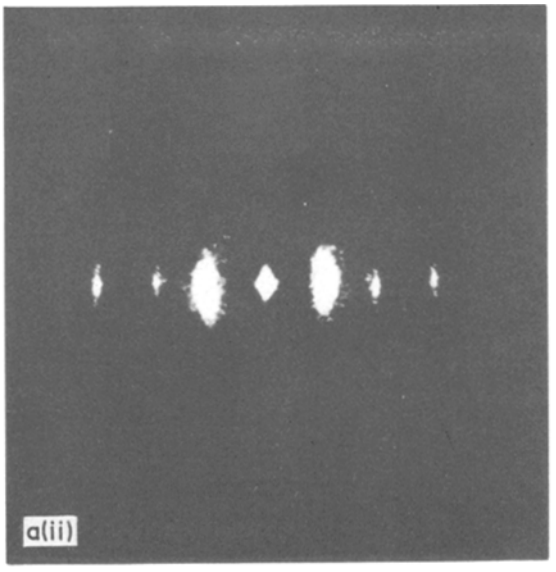

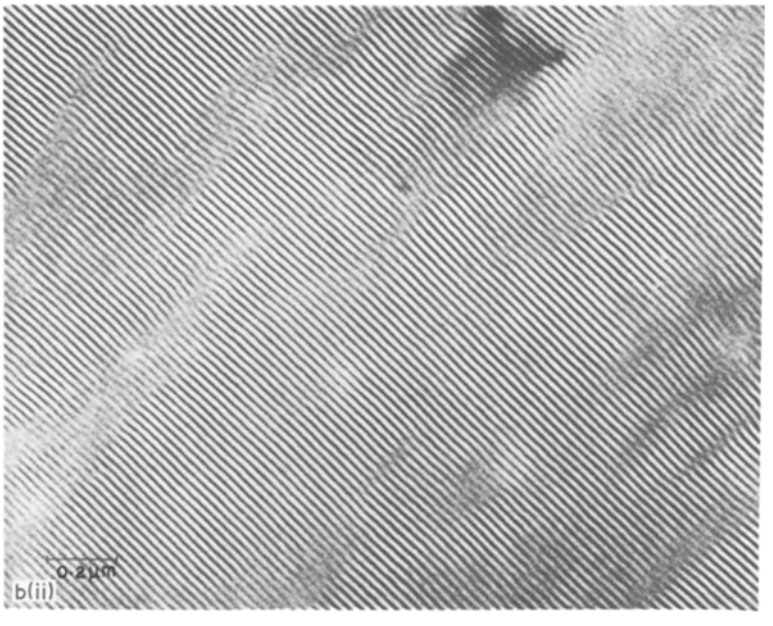

Figure 11 Continued.

by the work of Maurer [112] on crystal nucleation in titania-containing glasses. Light-scattering measurements were used firstly to detect the presence of scattering centres and study the initial stages of crystal nucleation, and secondly to estimate the average crystal size and concentration so that the crystallization process could be followed and the crystal-growth rate measured. The three important parameters which were measured were Rayleigh's ratio, the dissymmetry coefficient (the ratio of the intensities of scattering at angles symmetrical about the 90° position) and the degree of depolarization (the ratio of light intensities of vertical and horizontal polarization scattered at 90°). Measurements on the glass before heat-treatment showed that the scattering was about three times as high as that which would be expected from the refractive index and the depolarization was about one-third of the expected value. These results suggested that a glass-in-glass type phase separation had occurred during the preparation of the titania-containing

glass. On heat-treatment at the lowest temperature (725° C) there was initially a six-fold increase in depolarization without any change in dissymmetry and only a 30% increase in total scattering. This indicated that the scattering centres were becoming anisotropic and it was concluded that crystallization was taking place within the glass particles. The growth of the crystalline centres as a result of heat-treatment was followed by measurement of the average particle size. This was deduced from measurements of Rayleigh's ratio and the volume concentration of the particulate phase using a theory developed by Maurer which indicated that, if the number of crystalline particles remained constant, the crystal diameter should vary as the sixth root of the Rayleigh ratio. The volumetric concentration of the crystals was obtained from the integrated intensity of an X-ray diffraction line and this was then used to obtain the crystal diameter from the Rayleigh ratio. Crystal diameters of from 70 to 175 Å obtained by this method were in good agreement with those obtained from X-ray line broadening measurements.

Light-scattering behaviour has also been shown to depend on the domain size in phase-separated borosilicate glasses [113] and on spherulite size in films of polyethylene [114, 115].

Periodicity in a composite structure can result in diffraction effects if the wavelength of the incident light is of the same order as the composite period λ. The behaviour of the aligned lamellar Co_2Si–Co eutectoid [10] is given as an example by Albers [1]. By preferentially etching the surface of a specimen in which λ was equal to 0.5 μm, a periodic relief structure of the ridge type was obtained which showed diffraction spectra when illuminated with white light. The diffraction patterns obtained by optical reflection from the polished and etched surfaces of directionally solidified eutectic alloys have been discussed by Clarke [116] who has shown how they may be used for the detection of surface symmetries and for the measurement of interparticle spacing.

The spacing between the NaF rods in an NaCl–NaF eutectic has been obtained by reflecting laser light from the polished surface of a transverse section and measuring the distance to the first diffraction ring [117]. Similarly, in low-angle X-ray diffraction studies of an extruded SBS (polystyrene–polybutadiene–polystyrene) block co-polymer, it was found that sharp single-crystal diffraction patterns possessing hexagonal symmetry were obtained [118] and it was shown both from the X-ray and electron microscopic evidence [119] that the material consisted of polystyrene cylinders embedded in a polybutadiene matrix with the cylinder axes along the extrusion direction. The polystyrene rods were 150 Å in diameter and arranged in a hexagonal lattice with a lattice parameter of 300 Å. The low-angle X-ray diffraction patterns [118] are shown in Fig. 11a and the electron micrographs [119] in Fig. 11b. This X-ray and electron microscope evidence has been used for the interpretation of the mechanical properties of "single crystal" samples of SBS co-polymer [120].

Sievers [117] has discussed the diffraction behaviour of dielectric eutectics and described results obtained in an investigation of the infra-red transmission of the NaCl–NaF eutectic. The longest wavelength incident on the crystal satisfying the diffraction condition for rods arranged in a hexagonal array would be expected to be given by

$$\lambda_{max} = \sqrt{3} n^* d, \tag{80}$$

where λ_{max} is the wavelength of the incident light, n^* the effective refractive index and d the spacing between nearest neighbours. The agreement between the calculated value for λ_{max} and the experimental value for strong absorption was within 5% for $d = 4.5\,\mu$m and within 2% for $d = 5.8\,\mu$m.

Provided the periodicity is very much less than the wavelength of the light, a composite material containing aligned elongated particles of an optically isotropic material in an optically isotropic matrix (with a different refractive index) will exhibit birefringence (or double refraction). This is a straightforward consequence of the anisotropic dielectric properties and the effective refractive indices can be calculated from e.g. Equations 25 and 26 using the relationship, $n^* = (\epsilon^*)^{1/2}$, between the effective refractive index n^* and the effective dielectric constant ϵ^*. For a material containing aligned cylinders it is then easily shown [117] that

$$n_e^* = (V_1\epsilon_1 + V_2\epsilon_2)^{1/2} \tag{81}$$

and

$$n_0^* = \left\{\epsilon_2\left[\frac{\epsilon_2(1-V_1)+\epsilon_1(1+V_1)}{\epsilon_2(1+V_1)+\epsilon_1(1-V_1)}\right]\right\}^{1/2} \tag{82}$$

and the composite behaves as a uniaxial material with the optic axis along the cylinder axis.

Composite systems containing aligned metallic rods in a semiconductor or an insulator can also act as polarizing filters when the diameter of the rods is small compared with the wavelength. With the unidirectionally solidified InS–NiSb eutectic the rod diameter is typically about 0.5 μm and with a layer 70 μm in thickness the polarizability at wavelengths above 12 μm is at least 0.99. Electromagnetic waves with an electric vector vibrating parallel to the axis of the rods lose energy and transverse the composite with reduced amplitude. A wave with an electric vector perpendicular to the rods will, however, be damped very little [7].

The behaviour in the microwave region of artificial dielectrics consisting of a lattice of conducting elements or an array of elements of one permittivity embedded in a dielectric of a different permittivity has been discussed by Brown [121].

3.2. Magnetic properties

In a ferromagnetic material, at temperatures well below the Curie point, the electronic magnetic moments will be aligned within small contiguous regions – magnetic domains – within each of which the local magnetization is saturated. In the demagnetized state, the directions of magnetization in the different domains will vary so that the overall magnetization is zero. On applying a magnetic field, the magnetic moment can increase, firstly by an increase in the volume of the domains which are favourably oriented with respect to the field and secondly, in stronger fields, by rotation of the magnetization. The high coercivity required in permanent magnets is achieved by suppressing the possibility of domain boundary displacement. This can be accomplished by using very fine particles. A particle with a diameter less than about 0.1 to 0.001 μm will always be magnetized to saturation since the formation of a flux-closure configuration will be energetically unfavourable [122]. Magnetization reversal cannot take place in a sufficiently small single domain particle by boundary displacement. It can only take place by rotation of the magnetization so that large fields (depending on the anisotropy energy and shape of the particle) may be required.

The cast or sintered alloys of iron, aluminium, nickel and cobalt have been the most widely used materials for permanent magnets. Recently, however, fine-particle permanent magnet materials based on cobalt–rare earth alloys have been developed which have properties superior to any previously known [123]. The general properties of the Alnicos and other cobalt alloy permanent magnets have been reviewed by Gould [124].

In recent years considerable attention has been given to the investigation of rod-type eutectics, obtained by unidirectional solidification, as permanent magnet materials since, in the absence of magnetocrystalline anisotropy, the magnetic particles need only be small in two dimensions and, as a consequence of the shape anisotropy of the demagnetization energy, can be large in the third dimension. This is the concept of the "elongated single domain".

Progress in this field has been reviewed by Galasso [3, 40], Albers [1] and Sahm and Hofer [125]. A number of eutectic components containing magnetic rods in a non-magnetic matrix have been investigated including InSb – MnSb [126], FeS–Fe [127], Bi–Co [125] and Sb–MnSb [128]. Livingston [129] in studies with the Au–Co eutectic found that as the diameter of the Co–rods fell from 1 μm to 0.07 μm, the coercive force along the rod axes increased from 30 to 330 Oe. In early work on the directionally solidified Bi–MnBi system, Noothoven van Goor and Zijlstra [130] obtained a value of 11 kOe for the coercive force at room temperature. In more recent work [131] values as high as 24 kOe have been obtained with MnBi rod diameters of around 0.5 to 1.0 μm. With material containing rods of smaller diameter the coercive force decreased. This was thought to be due to an increasing lack of alignment in material obtained at very high growth rates. Although these materials exhibit a high coercive force the volume fraction of magnetic rods and the energy product is low. As noted by Albers [1], the best magnetic *in situ* composites are still probably the Alnico alloys obtained by spinodal disproportionation [132]. These contain a high volume fraction of ferromagnetic rods and have a high energy product (11×10^6 GOe).

Several eutectic systems with magnetic rods in a magnetic phase have been investigated including CoSb–Co [125], Y_2Co_{17}–Co [3], and Sm_2Co_{17}–Co [125]. With the latter system which contained ferromagnetic Co–rods in a ferromagnetic Sm_2Co_{17} matrix, Sahm and Hofer found that the coercive force increased from 50 to 500 Oe as the rod diameter was decreased from 2 μm to 0.2 μm.

For soft magnetic materials, fine particle sizes have to be avoided. Work on Co–Nb and Co–Nb–Fe directionally solidified eutectics with soft magnetic properties has been described by Colling and Kossowsky [133, 134].

3.3. Superconducting properties

The boundaries of the superconducting state are defined by the critical temperature T_c and, in a magnetic field, by the critical field $H_c(T)$ at which the magnetic flux penetrates the specimen and the superconductivity is destroyed. With type I superconductors the flux penetrates abruptly at H_c; with type II superconductors penetration occurs gradually over a range H_{c1} to H_{c2}. With thin films in which the thickness is very much less than the London penetration depth (typically about 500 Å), there is no Meissner effect and the critical field H_c can be very high. In a composite superconducting material the value of H_c can, therefore, increase when the dimensions of the superconducting phase are sufficiently small. This effect is illustrated by the work of Watson [135, 136] on porous glass impregnated with indium. With pore diameters of from 65 to 250 Å and at a temperature T below $T/Y_c = 0.5$, the critical field H_c was given by

$$H_c = (3415 \pm 40)\,[1-(T/T_c)^2]\,/d^{1.00\,\pm\,0.14} \tag{83}$$

where d is the pore diameter in Å so that, at a given temperature, the critical field was approximately inversely proportional to the pore diameter. Small increases in T_c have also been reported with systems of this type [136], the greatest relative effect being obtained with an Al–Al_2O_3 multilayer structure in which T_c was 4.5° K compared with a value of 1.2° K for Al [137]. When both phases are metallic decreased phase dimensions are likely to lead only to decreased critical fields [138].

At present, the main application of filamentary superconducting composites is in the construction of powerful electromagnets in which one of the main problems is that of stability [139, 140]. Instability in the shielding currents induced in the superconductor can lead to the phenomenon known as flux-jumping. The conditions required to achieve stability have been summarized and examined in a series of papers by Wilson and his colleagues [141–145]. To achieve adiabatic stability, the energy dissipated by a perturbation is reduced to a level at which it can be absorbed by the material itself without a serious rise in temperature which would lead to destruction of the superconductivity. The criterion for adiabatic stability is given by the relation [146, 147].

$$x < (10^9 \pi S T_0)^{1/2}/4J_c \tag{84}$$

where x is the penetration depth of the magentic field (cm), S is the heat capacity (J cm^{-3} K^{-1}),

$$T_0 = J_c/(-\mathrm{d}J_c/\mathrm{d}T), \tag{85}$$

and J_c is the current density (A cm^{-2}). This relation gives the approximate thickness of superconductor below which flux jumping should not occur. Typical numerical values for the type II superconductor NbTi are $S \sim 2 \times 10^{-3}$, $T_0 \sim 4$ corresponding to a superconductor thickness or filament diameter of about 0.008 cm for a J_c of 3×10^5 A cm^{-2}.

An alternative approach is to slow down the motion of flux by incorporating a low resistivity normal metal (e.g. Cu) thus allowing time for the heat to escape from the superconductor by thermal conduction. The corresponding dynamic stability criterion is given, for a composite consisting of alternate layers of superconductor and normal metal (e.g. Cu), by the relation [148–150]

$$d^2 \leqslant 8\,\frac{T_0 K_s}{\rho}\,\frac{1-\lambda_s}{\lambda_s}\,\frac{1}{J_c^2}, \tag{86}$$

where d is the thickness of the superconductor (cm), T_0 is given by Equation 85, k_s is the thermal conductivity of the superconductor (W cm^{-1} K^{-1}), ρ is the resistivity of the normal metal (Ωcm) and λ_s is the volume fraction of superconducting material. This relation gives similar values for the superconductor thickness (or filament diameter) to those given by Equation 84. For example, with $T_0 \sim 4$ K, $J_c \sim 3 \times 10^5$ A cm^{-2}, $k_s \sim 10^{-3}$ W cm^{-1} K^{-1}, $\rho \sim 2 \times 10^{-8}$ Ωcm and $\lambda \sim 0.5$, we find that $d \leqslant 0.004$ cm. Wilson *et al.* consider, however, that adiabatic stability (which assumes no heat loss during a perturbation) provides the more secure basis for achieving reliable superconducting performance.

A.c. losses in filamentary superconductors also depend on filament diameter and the calculation of these losses has been discussed by London [151], Hancox [152] and Wipf [153]. Wilson *et al.* have summarized the basic formulae for losses in coils [141].

Since the satisfactory performance of filamen-

tary superconductors is dependent on a fine filament diameter continued attention has been given to the superconducting properties of directionally solidified eutectics. References to the earlier work are given in the reviews by Galasso [3] and by Gallaso *et al.* [4]. Recent work has included re-examinations of the superconducting properties of unidirectionally solidified Pb–Sn eutectics [154, 155] together with a preliminary investigation [155] of the Josephson effect at 4.2 K with different interlamellar spacings.

3.4. Heat transfer

In the earlier discussion of the thermal conductivity of composite materials (Sections 2.4) it was assumed that (a) interface effects were absent and (b) heat transfer by radiation did not occur. We now consider conditions under which these two assumptions are no longer valid and the heat transfer properties become dependent on phase dimensions.

Heat can be carried through a solid by electrons, lattice waves (phonons), magnetic excitations or electromagnetic radiation (photons). The thermal conductivity (λ) of the solid is given by

$$\lambda = \tfrac{1}{3} \sum C_i v_i l_i, \tag{87}$$

where i is the type of carrier, C_i is the contribution of the carrier to the specific heat, v_i is the carrier velocity, and l_i is the mean free path of the carrier.

If the dimensions of the specimen are sufficiently small, the mean free path of a carrier will not be the same as that in the bulk material but will be limited by the external boundaries of the specimen. The thermal conductivity will then no longer be an intrinsic property but will depend on the specimen dimensions.

With dielectric crystals, for example, where the phonon free paths can be long at low temperatures the thermal conductivity is given by

$$\lambda(T) = \tfrac{1}{3} C(T) v L \tag{88}$$

where L is of the order of the shortest linear dimension of the specimen, C is the specific heat, and v is the velocity of the lattice waves (or the sound velocity). The temperature dependence of λ will then parallel that of the specific heat due to lattice waves and $\lambda(T)$ will vary as T^3 at the lowest temperatures.

In a polycrystalline aggregate, the phonon mean free path can be determined by the size of the individual grains or crystallites. If these are of the order of tens of microns this can lead to a depression in $\lambda(T)$ at low temperatures and an extension of the region in which $\lambda(T)$ is proportional to $C(T)$ to higher temperatures than with single crystals.

There is, therefore, a size effect which may have to be taken into account in considering heat transfer in composite materials at low temperatures. There may also be an interface effect since acoustic mismatch can limit the transmission of phonons across the boundary and there will then be a finite difference between the temperature on one side of the interface and that on the other (With metals and liquid helium this is known as the Kapitza thermal boundary resistance). A theoretical treatment of this effect has been given by Little [156] who showed that for a perfect junction with zero modulus of rigidity in both materials, the net flow of heat across the interface at low temperatures from material 1 to material 2 is given by

$$\frac{d\phi}{dt} = 5.01 \times 10^{16} \frac{\Gamma A}{C_1^2} (T_1^4 - T_2^4) \text{erg sec}^{-1}, \tag{89}$$

where Γ is a complicated function of the densities of the two materials and the ratio of the acoustic velocities, A is the area of the interface, C_1 is the group velocity (cm sec^{-1}) of the longitudinal phonons in the first material, and T_1 and T_2 are the temperatures (K) in the two materials. For small values of $(T_1 - T_2)/T_1$. Equation 89 can be written in the form

$$\frac{d\phi}{dt} \approx 2.0 \times 10^{17} \frac{\Gamma A}{C_1^2} T_1^3 \Delta T \text{ erg sec}^{-1}, \tag{90}$$

so that the boundary resistance is inversely proportional to T^3. At low temperatures the effects of this boundary resistance can become very pronounced. The addition of a fine metal powder to a dielectric would for example, be expected to increase the thermal conductivity. However, at low temperatures, the temperature dependence of the boundary resistance can exceed that of the thermal resistance of the dielectric and the thermal conductivity of the composite will then be *less* than that of the dielectric [157].

These effects have been investigated by Garrett and Rosenberg [158] who measured the thermal

TABLE VI Matrix of properties (after van Suchtelen [8]. The table classifies the physical properties or phenomena in materials according to the kind of input parameter (columns) and output parameter (rows).

Y	X					
	(1) Mechanical $K/\Delta l$	(2) Magnetic: H/M	(3) Electrical: $E/P, i$	(4) Optical and particle radiation: light or particle flux	(5) Thermal: T, grad T, heat current	(6) Chemical: (grad) C, (grad) μ
(1) Mechanical: $K/\Delta l$	elasticity	(i) magnetostriction (ii) magnetoviscosity (suspensions)	(i) electrostriction (i) Kirkendall effect (iii) electroviscosity (suspensions) (iv) indirect: thermal expansion	–	thermal expansion	osmotic pressure
(2) Magnetic H/M	piezomagnetism	x	(i) superconductors (ii) galvanic deposition of FM layer (iii) direct generation of magnetic field	photomagnetic effect	$\{+ H\}$ ferromagnetic material at $T \simeq T_c$	dependence of T_c on C (FM)
(3) Electrical: $E/P, i$	(i) piezoelectricity (ii) piezoresistivity	(i)$\{+ i\}$ magnetoresistance (ii)$\{+ i\}$ Hall effect (iii) a.c. resonance (iv) induction of voltage	ϵ, p $\{+ H\}$ Hall effect	(i) photoconductivity (ii) photo-emission (iii)$\{+ H\}$ PEM effect (iv) ionization	(i) thermoelectric (ii)$\{+ E\}$ ferroelectrics at $T \simeq T_c$ (iii)$\{+ i\}\ \rho(T)$	dependence of T_c on C (FE)
(4) Optical and particles: light or particle flux	(i) stress birefringence (ii) triboluminescence	(i) Faraday effect (ii) magneto-optic Kerr effect (iii) deflection of charged particles	(i) electro luminescence (ii) laser junctions (iii) n (iv) Kerr effect (v) absorption by galvanic deposits (vi) cold emission of electrons	n fluorescence scintillation colour-centre activation	thermoluminescence	chemoluminescence

TABLE VI continued.

Y	X					
	(1) Mechanical: $K/\Delta l$	(2) Magnetic: H/M	(3) Electrical: E/P, i	(4) Optical and particle radiation: light or particle flux	(5) Thermal: T, grad T, heat current	(6) Chemical: (grad) C, (grad) μ
(5) Thermal: T, grad T, heat current	(i) heat of transition of pressure-induced phase transition (ii) piezorestivity and Joule heating	(i) adiabatic demagnetization (ii) $\{+ i\}$ grad T NE effect (iii) $\{+ E\}$ magnetoresistance effect + Joule heating	(i) dissipation in resistance (ii) Peltier effect (iii) $\{+ H\}$ grad T NE effect	absorption	λ	reaction heat
(6) Chemical: (grad) C, (grad) μ	pressure-induced phase-transition	–	(i) electromigration (ii) galvanic deposition	light or particle stimulated reactions (photosensitive layers)	(i) Soret effect (grad T) (ii) phase transition (iii) change of chemical equilibrium	–

Symbols

C chemical composition, concentration
E electric field
H magnetic field
i electric current
K (mechanical) force
Δl deformation
M magnetic polarization
n refractive index
P dielectric polarization
T temperature
ϵ dielectric constant
x magnetic susceptibility
λ thermal conductivity
μ chemical potential
ρ resistivity
FM ferromagnetic
FE ferroelectric
NE Nernst–Ettingshausen

Bracket symbols, e.g. $\{+ i\}$, indicate that the parameter represented by the symbol in the brackets is essential as a second input (e.g. i and H in the Hall effect).

conductivities of epoxy resin composites at temperatures between 2 and 300 K. The fillers included glass spheres and quartz, corundum and diamond powders. The quartz and diamond particles were irregular in shape; the corundum particles were in the form of small platelets. Above about 10 to 20 K, the results with the epoxy/glass composites were in agreement with a modified form of the Rayleigh equation derived by Meredith and Tobias [159], with the quartz and diamond powders the results were interpreted using the Hamilton and Crosser equation for thermal conductivity [160] which includes a shape parameter. With all the samples the thermal conductivity above 20 K was found to be higher than that of the unfilled rasin and to increase with increasing filler concentration.

Below 20 K, marked changes in the composite conductivity were observed and with some samples the thermal conductivity was appreciably lower than that of the unfilled resin. The thermal conductivity in the liquid helium region was also strongly dependent on the size of the particles and this dependence could not be explained merely in terms of a frequency-independent scattering of phonons at the particle boundaries. Garrett and Rosenberg considered that this discrepancy was due to acoustic mismatch at the matrix–particle interface and showed that the low temperature results could be interpreted by calculating an effective thermal conductivity for the filler particles based on measurements of thermal contact resistance.

At high temperatures, the effects of radiative heat transfer may have to be considered. With a material which is partially transparent each volume element will absorb part of any incident radiation and will also re-radiate energy. A certain amount of energy can therefore be transmitted through the material by these processes of absorption and re-radiation in addition to that conducted by lattice waves. When the thickness of the specimen is much larger than the mean free path of the photons, the apparent radiative thermal conductivity will be proportional to T^3 and inversely proportional to the Rosseland mean extinction coefficient. When the specimen is optically thin, the apparent radiative thermal conductivity will again be proportional to T^3 but will also be proportional to the thickness so that the thermal conductivity is no longer an intrinsic property of the material [161].

With composite materials, the photons will be scattered at the phase interfaces but, assuming the photon mean free path is independent of frequency the thermal conductivity due to radiation will again be proportional to T^3. The effects of a frequency dependence of the mean free path on radiative heat transfer through composite materials have been considered by Klemens and [162]. At low frequencies the mean free path must be strongly frequency dependent and indeed if the particles are small compared to the wavelength, the mean free path should vary as $1/\nu^4$. Long-wavelength photons can, therefore, play an important part in heat transfer through composite materials such as polycrystalline solids, densely packed powders, foams and fibrous aggregates with the result that the radiative thermal conductivity at moderately high temperatures may be very much higher than would be expected from extrapolating down from temperatures above 2000 K according to a T^3 law.

4. Product properties

The concept of product properties was first described by van Suchtelen [8] and has also been discussed by Albers [1]. These properties can be distinguished from most of the material property combinations considered in the previous sections since they depend on the way in which the behaviour of one phase affects that of another.

Most physical properties of materials can be defined in terms of an X–Y effect in which X is an input parameter and Y a corresponding output parameter. As we have noted, the behaviour of the material is then described in terms of a proportionality tensor $\partial Y/\partial X = A$ where A is a property such as electrical conductivity or magnetic susceptibility. Van Suchtelen distinguished two ways in which material properties can be combined in a two-phase composite material:

(a) The property arising from an X–Y effect in material 1 can be combined with that from an X–Y effect in material 2. Together these give an X–Y effect in the composite. These properties which were termed "sum properties" by Van Suchtelen have been discussed in the previous sections.

(b) The output from an X–Y effect in material 1 can form the input for a Y–Z effect in material 2 to give an X–Z effect in the composite material. The corresponding properties were termed "product properties" by van Suchtelen.

TABLE VII Product properties of composite materials (after van Suchtelen [8])

$X-Y-Z$ (Table II)	Property of phase I $X-Y$	Property of phase II $X-Y$	Product property $X-Z$
123	piezomagnetism	magnetoresistance	piezoresistance; phonon drag
124	piezomagnetism	Faraday effect	rotation of polarization by mechanical deformation
134	piezoelectricity	electroluminescence	piezoluminescence
134	piezoelectricity	Kerr effect	rotation of polarization by mechanical deformation
213	magnetostriction	piezoelectricity	magneto-electric effect
213	magnetostriction	piezoresistance	magnetoresistance; spin-wave interaction
253	Nernst-Ettingshausen effect	Seebeck effect	quasi-Hall effect
214	magnetostriction	stress-induced birefringence	
312	electrostriction	piezomagnetism	magnetically induced birefringence
313	electrostriction	piezoresistivity	electromagnetic effect
343	electroluminescence	photoconductivity	coupling between ρ and E (negative diff. resistance, quasi Gunn effect)
314	electrostriction	stress-induced birefringence	electrically induced birefringence;
421	photomagnetic effect	magnetostriction	light modulation
421	photoconductivity	electrostriction	photostriction
434	photoconductivity	electroluminescence	wavelength changer (infra-red visible etc)
443	scintillation	photoconductivity	radiation induced conductivity (detectors)
444	scintillation fluorescence	fluorescence	radiation detectors 2-stage fluorescence

The concept of product properties is clearly of considerable potential importance in the development of composite materials with novel properties. The principle may be similar to that in an electronic or other device but with the composite material the resulting property is an intrinsic property of the material. The $X-Z$ effect may be achieved by the use of different Y parameters and the coupling mechanism can consequently take different forms: electrical, optical, magnetic, thermal, chemical and mechanical coupling are all possibilities. An example of mechanical coupling would be a magneto-electric effect produced in a composite material by mechanical coupling between a magnetostrictive phase and a piezoelectric phase.

The potentialities of this concept are illustrated by Tables VI and VII taken from the paper by van Suchtelen. Table VI is essentially a 6 x 6 matrix in which the most obvious $X-Y$ (or $Y-Z$) effects have been tabulated. These can then be combined as indicated in Table VII to give the product properties listed in the table.

The feasibility of this approach has been confirmed experimentally by (a) the investigation of magneto-electric and electromagnetic effects in a $BaTiO_3-CoFe_2O_4$ eutectic and (b) the development of an X-ray fluorescent material consisting of fine ($\simeq 1\,\mu m$) $PbCl_2$ particles in an anthracene matrix. In the latter case, the X-rays release secondary electrons with high efficiency in the $PbCl_2$ and these electrons which have a range of a few μm spend most of their time in the anthracene which is a good scintillator. The composite had an X-ray to visible light conversion efficiency exceeding that of anthracene (saturated with $PbCl_2$) by at least one order of magnitude in a layer thickness less than 0.05 cm.

In a sense, product properties can be regarded as a special, and potentially important, aspect of the general physical behaviour of composite materials. In the general case, when considering the physical behaviour of a composite material all the possible interactions between the phases should considered whether they be electrical, magnetic or mechanical. This is not usually done and in the consideration of dielectric properties it is normally assumed that mechanical interactions are absent and that piezoelectric effects do not have to be considered. On the other hand, in the discussion of thermal expansion it is recognized that mechanical interactions must be important and these are taken

into account. The concept of product properties is, however, of considerable importance since it indicates the ways in which interactions arising through different forms of coupling can be exploited in the development of materials with novel properties.

5. Other special property combinations

As we have seen, a particular property of a composite material can be varied in a controlled way by controlled changes in the composition and structure. This means that by a suitable selection of components and structural geometry it may be possible to achieve a combination of properties which cannot be realized with a homogeneous material. Thus, for example, with fibre composites we have the possibility of very high mechanical strength combined with very high electrical conductivity.

The possibility of achieving a particular combination of physical properties is illustrated by the work of Liebmann and Miller [163] on the thermoelectric properties of directionally solidified InSb–Sb eutectics. The microstructure consisted of antimony rods in an InSb matrix. Values for the specific resistance (ρ), the thermoelectric power (ϕ) and the thermal conductivity (K) are given in Table VIII which also includes values for the figure of merit (Z) given by

$$Z = \frac{\phi^2}{\rho K}.$$

It follows from equation 91 that a reduction in the thermal conductivity will lead to a higher value for Z and with semi-conductors this can be achieved by mixed crystal formation which leads to statistically distributed lattice distortions [7].

It will be seen from Table VIII that the InSb–Sb eutectics are markedly anisotropic in electrical resistance and that the values of ϕ and K differ considerably from those for the pure materials. Unfortunately, the values of Z are not as high as the values for either InSb or Sb although higher values might be obtained by a further reduction in rod diameter. Similar studies have been carried out with the Bi_2Te_3–Te [3], Mg–$Mg_{17}Al_{12}$ and Bi–Cd [164] systems but the figure of merit values with these materials were not sufficiently outstanding to make them competitive with single phase materials [3]. More recently Levinson [165] has examined the thermoelectric properties of an aligned $CrSi_2$–Si eutectic.

The outstanding example of the way in which a required combination of electrical properties can be achieved with a composite material is provided by the development at the Siemens Laboratories of magnetoresistive devices based on the directionally solidified InSb–NiSb eutectic in which metallic NiSb rods are aligned in a InSb matrix (Fig. 12). This work has been summarized recently

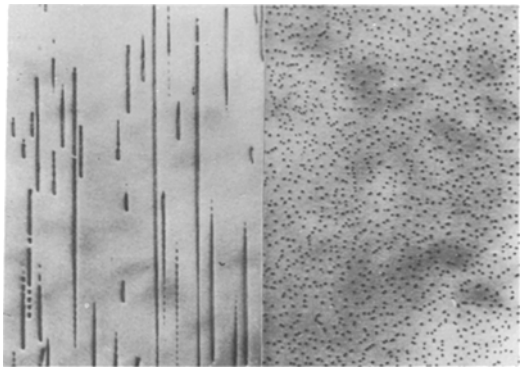

Figure 12 Polished surface of InSb–NiSb eutectic. Left: surface parallel to NiSb needles. Right: surface perpendicular to NiSb needles [7]. (Courtesy Professor H. Weiss.)

TABLE VIII Thermoelectric properties of directionally solidified InSb–Sb eutectics [163]

Sb rod size (cm)	Direction of measurement (to Sb rods)	ρ (Ωcm)	ϕ (μV deg^{-1})	K (W cm^{-1} deg^{-1})	$Z \times 10^6$ (deg^{-1})
4.3×10^{-4}	$\parallel$	3.05×10^{-4}	-18	0.1113	9.5
	$\perp$	3.3×10^{-3}	-71	0.0822	18.6
8.5×10^{-4}	$\parallel$	3.00×10^{-4}	-12	0.1235	3.9
	$\perp$	3.3×10^{-3}	-53	0.0940	9.1
2.8×10^{-3}	$\parallel$	3.15×10^{-4}	-8.2	0.1430	1.5
	$\perp$	3.4×10^{-3}	-28	0.1059	2.2
Pure materials					
InSb		10^{-2}	-325	0.162	65.2
Sb		4.4×10^{-5}	$+35$	0.189	147.3

by Weiss [7] and will only be discussed briefly in this review.

The origin of the large magnetoresistive effect in these materials can be explained by first considering the Hall effect in an elongated plate of InSb traversed by a current i flowing in a direction parallel to the longitudinal axis of the plate. If a magnetic field B is applied in a direction perpendicular both to the plane of the plate and the direction of the current then a Hall voltage perpendicular to I and B is obtained. If the Hall voltage is now short circuited by wires at intervals along the plate as shown in Fig. 13a, then the Hall current flowing through these wires produces a further Hall voltage parallel to the primary current i and results in an additional resistance ΔR which will be proportional to the magnetic field. The current flowing through the InSb will follow a zig-zag path from one end of the plate to the other. With an infinite number of short circuits, the relative increase in resistance will be $(\mu_B B)^2$ where μ_B is the electron Hall mobility in a magnetic field B. For intrinsic InSb, $\mu_B B$ has a value of 5 in a field of 10 kG so that a 25-fold increase in resistance should be theoretically attainable with a short circuited material.

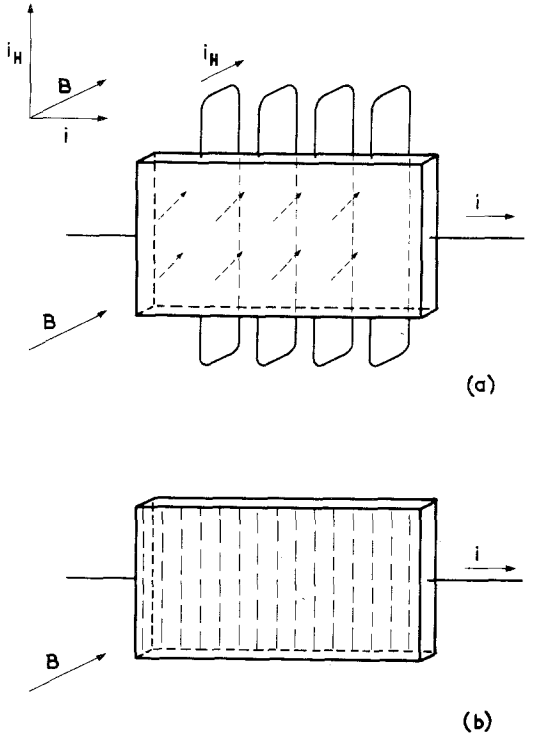

Figure 13 Magnetoresistive effect in directionally solidified InSb–NiSb eutectic. (a) Externally short circuited InSb plate. (b) Short-circuiting NiSb needles in InSb–NiSb eutectic. (After Weiss [71.)

In the InSb–NiSb eutectic the short circuits are provided by the metallic NiSb rods (Fig. 13b) which have an electrical conductivity two orders of magnitude greater than that of the InSb matrix. With the aligned eutectic about 60% of the theoretical magnetoresistive effect is obtained. The more important applications of magnetoresistive devices based on the InSb–NiSb eutectic include the measurement of magnetic fields, contactless variable resistances and potentiometers (Fig. 14), and other contactless controls.

Figure 14 Contactless nominal current indicator for electric locomotive brake (courtesy Professor H. Weiss).

In a sense, the InSb–NiSb eutectic could be regarded as a device rather than a material. However, as noted by Albers [1], the composite is essentially a new material showing an extremely high magnetoresistance effect and this property is retained whatever the shape of the specimen. The effects arise through a special anisotropic combination of the electrical properties of InSb and NiSb. A similar high magnetoresistive effect would be shown by InSb itself if the electron and hole mobilities were equally high. In fact the hole mobility in InSb is small. The composite is, therefore, essentially a new material with unique properties.

In addition to the magnetoresistive effect the Hall current flowing through the NiSb rods gives rise to a Peltier effect so that a temperature difference is observed between the two surfaces of the eutectic. Unfortunately, although the figure of merit is 30 times as high as that of homogeneous InSb, the thermal conductivity of InSb is too high

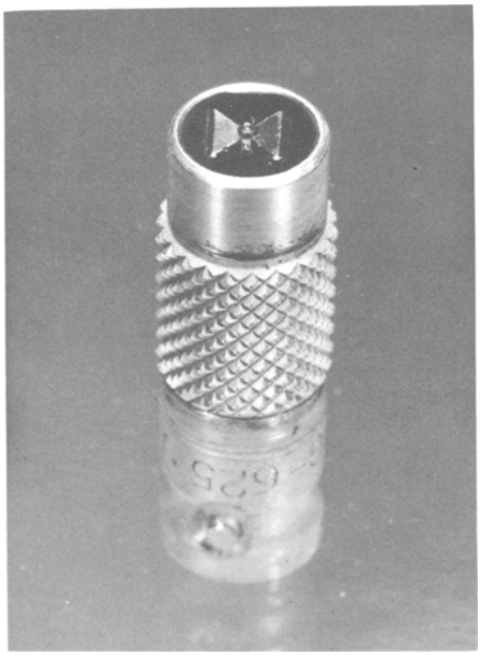

Figure 15 Infra-red detector with InSb–NiSb eutectic (courtesy Professor H. Weiss).

for devices based on this effect to have practical value. The converse effect which is observed when a temperature difference ΔT is imposed on the system has, however, been exploited in a room-temperature detector for the far infra-red (Fig. 15).

A large number of aligned eutectics involving III–V compounds have been examined [7] but none of these has shown the outstanding properties of the unidirectionally solidified InSb–NiSb system. A magnetoresistive effect was observed with the Cd As–NiAs eutectic [166] but again this was not as large as that with InSb–NiSb.

Acknowledgements

The author is grateful to the Director of the National Physical Laboratory for permission to publish this paper and is indebted to Professor A. Keller, Professor H. Weiss, Dr J. Dlugosz and Dr. W. Finger for their help in providing illustrations.

References

1. W. ALBERS, Proceedings of the Conference on *In Situ* Composites, September 5–8 (1972), Lakeville, Connecticut, Vol. III (Publication NMAB 308–III, Nat. Acad. Sci., Washington, D.C. 1973), pp. 1–19.
2. M. B. BEVER, P. E. DUWEZ and W. A. TILLER, *Mat. Sci. Eng.* **6**, (1970) 149.
3. F. S. GALASSO, *J. Metals* **19** (6) (1967) 17.
4. F. S. GALASSO, F. C. DOUGLAS and J. A. BATT, *J. Metals* **22** (6) (1970) 40.
5. Z. HASHIN, in "Mechanics of Composite Materials" (Proceedings of the 5th Symposium Naval Structural Mechanics, Philadelphia, Pa., May 8–10, 1967) edited by F. W. WENDT, H. LIEBOWITZ, N. PERRONE (Pergamon, 1970) pp. 201–242.
6. J. D. LIVINGSTON, *Composites* **4** (2) (1973) 70.
7. H. WEISS, *Met. Trans.* **2** (1971) 1513.
8. J. VAN SUCHTELEN, *Philips Res. Repts.* **27** (1972) 28.
9. W. F. BROWN, *J. Chem. Phys.* **23** (1955) 1514.
10. L. K. H. VAN BEEK, "Progress in Dielectrics", Vol. 7 (Heywood, London, 1967) pp. 69–114.
11. J. W. RAYLEIGH, *Phil. Mag.* **34** (1892) 481.
12. D. A. G. BRUGGEMAN, *Ann. Phys. Lpz.* **24** (1935). 636.
13. C. J. F. BÖTTCHER *Rec. Trav. Chim. Pays-Bas* **64** (1945) 47.
14. W. E. A. DAVIES, *J. Phys. D.* 7 (1974) 120.
15. D. POLDER, and J. H. VAN SANTEN, *Physica* **12** (1946) 257.
16. E. C. STONER, *Phil. Mag.* **36** (1945) 803.
17. Z. HASHIN, *J. Comp. Mater.* **2** (1968) 284.
18. O. WIENER, *Abh. sächs. Ges. (akad.) Wiss.* **32** (1912) 509.
19. W. F. BROWN, *Trans. Soc. Rheol.* **9** (1965) 357.
20. Z. HASHIN and S. SHTRIKMAN, *J. Appl. Phys.* **33** (1962) 3125.
21. J. A. REYNOLDS, Thesis (London 1955).
22. M. BERAN, *Il Nuovo Cimento* **38** (1965) 771.
23. P. B. CORSON, *J. Appl. Phys. (USA)* **45** (1974) 3159.
24. *Idem, ibid* **45** (1974) 3165.
25. *Idem, ibid* **45** (1974) 3171.
26. *Idem, ibid* **45** (1974) 3180.
27. M. N. MILLER, *J. Math. Phys.* **10** (1969) 1988.
28. J. J. McCOY, *Il Nuovo Cimento* **57B** (1968) 139.
29. J. M. PETERSON and J. J. HERMANS, *J. Comp. Mater.* **3** (1969) 338.
30. S. G. SPRINGER and S. W. TSAI, *ibid* **1** (1967) 166.
31. Z. HASHIN and B. W. ROSEN, *J. Appl. Mechs. (Trans. ASME)* **31** (1964) 223.
32. J. DONEA, *J. Comp. Mater.* **6** (1972) 260.
33. M. J. BERAN and N. R. SILNUTZER, *ibid* **5** (1971) 246.
34. M. A. ELSAYED and J. J. McCOY, *ibid* 7 (1973) 466.
35. J. C. MAXWELL, "A Treatise on Electricity and Magnetism", Vol. 1. 3rd Edn. (Clarendon Press, Oxford, 1892) p. 440.
36. R. LANDAUER, *J. Appl. Phys.* **23** (1952) 779.
37. S. M. AHARONI, *ibid* **43** (1972) 2463.
38. F. BUECHE, *ibid* **43** (1972) 4837.
39. *Idem, ibid* **44** (1973) 532.
40. *Idem, J. Polymer Sci., Polymer Phys. Ed. (USA)* **11** (1973) 1319.
41. J. GURLAND, in "Quantitative Microscopy" edited by R. T. De HOFF and F. N. RHINES (McGRAW–HILL, New York, 1968) pp. 278–290.

42. A. D. BRAILSFORD and K. G. MAJOR, *Brit. J. Appl. Phys.* **15** (1964) 313.
43. R. E. SKOCHDOPOLE *Chem. Eng. Prog.* **57(10)** (1961) 55.
44. A. W. PRATT, in "Thermal Conductivity", Vol. 1 edited by R. P. TYE (Academic Press, London, 1969) pp. 301–405.
45. A. SUGAWARA and Y. YOSHIZAWA, *J. Appl. Phys.* **33** (1962) 3135.
46. T. P. FIDELLE and R. S. KIRK, *A.I.Ch.E.J.* **17** (1971) 1427.
47. R. A. SCHAPERY and R. E. MARTIN, Mechanics and Materials Research Center, Texas A & M University Technical Report MM 72–2 (1972).
48. W. FINGER, *Schweiz Monatsschr, Zahnheilkd.* **84** (1974) 630.
49. V. M. LEVIN, *Mekhanika Tverdogo Tela* **1** (1967) 88.
50. B. W. ROSEN and Z. HASHIN, *Int. J. Eng. Sci.* 8 (1970) 157.
51. R. A. SCHAPERY, *J. Comp. Mater.* **2** (1968) 380.
52. J. L. CRIBB, *Nature* **220** (1968) 576.
53. T. R. STEEL, *Int. J. Solids Structures* **4** (1968) 1149.
54. Z. HASHIN, Proceedings of the IUTAM Symposium on Nonhomogeneity in Elasticity and Plasticity, Warsaw, Poland (Pergamon Press, New York, 1959) p. 463.
55. E. H. KERNER, *Proc. Phys. Soc. B.* **69** (1956) 808.
56. T. T. WANG and T. K. KWEI, *J. Polymer Sci. Part A2* 7 (1969) 889.
57. A. A. FAHMY and A. N. RAGAI, *J. Appl. Phys.* **41** (1970) 5108.
58. B. BUDIANSKY, *J. Mech. Phys. Solids* **13** (1965) 223.
59. *Idem, J. Comp. Mater.* **4** (1970) 286.
60. R. HILL, *J. Mech. Phys. Solids* **13** (1965) 213.
61. N. LAWS, *ibid* **21** (1973) 9.
62. B. PAUL, *Trans. Mct. Soc. AIME* **218** (1960) 36.
63. P. S. TURNER, *J. Res. NBS* **37** (1946) 239.
64. Z. HASHIN and S. SHTRIKMAN, *J. Mech. Phys. Solids* **11** (1963) 127.
65. R. HILL, *ibid* **11** (1963) 357.
66. L. J. WALPOLE, *ibid* **14** (1966) 151.
67. M. BERAN and J. MOLYNEUX, *Q. Appl. Mathematics* **24**(2) (1966) 107
68. J. J. McCOY, Recent Advances in Engineering Science Vol. VI. Ann. Meeting Conf. Eng. Sci., Nov. 1969, Princeton N.J. (1970) p. 235.
69. M. N. MILLER, *J. Math. Phys.* **10** (1969) 2005.
70. B. W. ROSEN, *Proc. Roy. Soc. Lond. A.* **319** (1970) 79.
71. G. A. VAN FO FY *Sov. Phys. Doklady* **11** (1966) **176**; *Doklady Akad, Nauk SSSR* **166** (1965) 817.
72. R. HILL, J. *Mech. Phys. Solids* **12** (1964) 199.
73. *Idem, ibid* **13** (1965) 189.
74. N. LAWS, *Int. J. Eng. Sci.* **12** (1974) 79.
75. W. SCHNEIDER, *Kunstoffe* **61** (1971) 273.
76. *Idem, ibid* **63** (1973) 929.
77. L. B. GRESZCZUK, AIAA Structures and Materials Conference 6th, Palm Springs, California 5–7 April 1965 (AIAA, New York, 1965) pp. 285–290.
78. B. W. ROSEN, in "Composite Materials", Agard Lecture Series No. 55, Advisory Group for Aerospace Research and Development, NATO (1972) pp. 1–1 to 1–22.
79. L. R. CALCOTE, "The analysis of laminated composite structures" (Van Nostrand–Reinhold, New York, 1969).
80. S. G. LEKHNITSKII, "Theory of elasticity of an anisotropic elastic body" translated by P. FERN, edited by J. J. Brandstatter (Holden–Day, San Francisco, 1963).
81. J. C. HALPIN and N. J. PAGANO, Technical Report AFML–TR–68–395, December 1969.
82. *Idem,* Technical Report AFML–TR–69–341, August 1970.
83. J. C. HALPIN, *J. Comp. Mater.* **6** (1972) 208.
84. N. F. DOW and B. W. ROSEN, NASA Report CR–1324, May 1969.
85. *Idem, Israel J. Technol.* 7 (1969) 209.
86. W. ALTHOF, Deutsche Forschungs- und Versuchsanstalt für Luft- und Rauhmfahrt eV. Institut für Flugzeugbau Report FD–44, October 1971.
87. A. A. FAHMY and A. N. RAGAI, *J. Appl. Phys.* **41** (1970) 5112.
88. D. E. GEILER, 28th Ann. Tech. Conf. SPI 1973, Reinforced Plastics/Composites Institute, The Society of Plastics Industry Inc, Section 9–D, pp. 1–8.
89. W. R. GOGGIN, *Appl. Optics* **13** (1974) 444.
90. A. A. FAHMY and A. N. RAGAI-ELLOZY, *J. Comp. Mater.* 8 (1974) 90.
91. J. C. HALPIN, *ibid* **3** (1969) 732.
92. C. C. CHAMIS, NASA Technical Note D–6696, March 1972.
93. J. SELSING, *J. Amer. Ceram. Soc.* **44** (1961) 419.
94. L. HOLLIDAY and J. ROBINSON, *J. Mater. Sci.* 8 (1973) 301.
95. L. E. NIELSEN, *J. Comp. Mater.* **1** (1967) 100.
96. G. A. COOPER and J. M. SILLWOOD, *J. Mater. Sci.* 7 (1972) 325.
97. T. C. HANSEN and K. E. C. NIELSEN, *J. Amer. Concrete Inst.* **62** (1965) 783.
98. G. PICKETT, *ibid* **27**(5) (1956) *Proceedings* **52** (1956) 581.
99. F. T. BARWELL and K. W. PEPPER, *Trans. Faraday Soc.* **42B** (1946) 275.
100. P. J. FLORY, "Principles of Polymer Chemistry" (Cornell University Press, Ithaca, New York, 1953) p. 576.
101. L. R. G. TRELOAR, "The Physics of Rubber Elasticity", 2nd Edn. (Clarendon Press, Oxford, 1958) p. 123.
102. A. Y. CORAN, K. BOUSTANY and P. HAMED, *J. Appl. Poly.* **15** (1971) 2471.
103. W. W. BARKAS, *Discuss. Faraday Soc.* **42B** (1946) 137.
104. I. D. CAVE, *Wood Sci. Technol.* **6** (1972) 157.
105. R. C. WYATT and K. H. G. ASHBEE, *Fibre Sci. Technol.* **2** (1969) 29.
106. K. H. G. ASHBEE and R. C. WYATT, *Proc. Roy. Soc. A.* **312** (1969) 553.
107. F. M. A. CARPAY and J. VAN DEN BOOMGARD, *Acta Met.* **19** (1971) 1279.

108. F. M. A. CARPAY and W. A. CENSE, *Scripta Met.* 8 (1974) 11.
109. F. W. PEAKER, in "Techniques of Polymer Characterization", edited by P. W. ALLEN (Butterworths, London, 1959) pp. 131–170.
110. P. DEBYE, *J. Phys. Chem.* **51** (1947) 18.
111. *Idem, J. Appl. Phys.* **15** (1948) 338.
112. R. D. MAURER, *ibid* **33** (1962) 2132.
113. L. PROD'HOMME, *Verres Refract.* **22** (1968) 604.
114. R. S. STEIN and M. B. RHODES, *J. Appl. Phys.* **31** (1960) 1873.
115. R. E. PRUD'HOMME and R. S. STEIN, *J. Polymer Sci., Polymer Phys. Ed. (USA)* **11** (1973) 1357.
116. D. R. CLARKE, *J. Mater. Sci.* **10** (1975) 172.
117. A. J. SIEVERS, Proceedings of the Conference on *In Situ* Composites, September 5–8 (1972) Lakeville, Connecticut, Vol. III (Publication NMAB 308–III, Nat. Acad. Sci., Washington, D.C. 1973) pp. 129–141.
118. A. KELLER, E. PEDEMONTE and F. M. WILLMOUTH, *Nature, Lond.* **225** (1970) 538.
119. J. DLUGOSZ, A. KELLER and E. PEDEMONTE, *Kolloid-Z. Z. Polym.* **242** (1970) 1125.
120. R. G. C. ARRIDGE and M. J. FOLKES, *J. Phys. D. (Appl. Phys.)* **5** (1972) 344.
121. J. BROWN, "Progress in Dielectrics", Vol. 2 edited by J. B. BIRKS and J. H. SCHULMAN (Heywood, London, 1960) pp. 193–225.
122. C. KITTEL, "Introduction to Solid State Physics", 3rd Edn. (Wiley, New York, 1966) p. 488.
123. J. H. WERNICK, *Ann. Rev. Mat. Sci.* **2** (1972) 607.
124. J. E. GOULD, "Cobalt Alloy Permanent Magnets", Cobalt Monograph Series 'Centre d'Information du Cobalt, Brussels, 1971).
125. P. R. SAHM and F. HOFER, *Z. Angew. Phys.* **30** (1970) 95.
126. H. WAGINI and M. WILHELM, *Z. Naturforschung* **21a** (1966) 329.
127. D. L. ALBRIGHT, G. P. CONRAD II and R. W. KRAFT, *J. Appl. Phys.* **38** (1967) 2919.
128. M. R. JACKSON, R. N. TAUBER and R. W. KRAFT, *J. Appl. Phys.* **39** (1968) 4452.
129. J. D. LIVINGSTON, *ibid* **41** (1970) 197.
130. J. M. NOOTHOVEN VAN GOOR and J. H. ZIJLSTRA, *ibid* **39** (1968) 5471.
131. J. C. BOULBES, R. W. KRAFT, M. R. NOTIS and C. D. GRAHAM, Proceedings of the Conference on *In Situ* Composites, September 5–8 (1972) Lakeville, Connecticut, Vol. III (Publication NMAB 308–III, Nat. Acad. Sci., Washington, D.C. 1973) pp. 61–78.
132. J. J. de JONG, J. M. G. SMEETS and H. B. HAANSTRA, *J. Appl. Phys.* **29** (1958) 297.
133. D. A. COLLING and R. KOSSOWSKY, *Met. Trans.* **2** (1971) 1523.
134. R. KOSSOWSKY and D. A. COLLING, "Science of Advanced Materials and Process Engineering", Vol. 15 (Society of Aerospace Material and Process Engineers – Western Periodicals, North Hollywood, California 1969) pp. 491–500.
135. J. H. P. WATSON, *Phys. Rev.* **148** (1966) 223.
136. *Idem, Phys. Letters* **25A** (1967) 326.
137. M. STRONGIN, F. KAMMERER, D. H. DOUGLASS, JUN. and M. H. COHEN, *Phys. Rev. Letters* **19** (1967) 121.
138. J. D. LIVINGSTON, *J. Appl. Phys.* **38** (1967) 2408.
139. B. J. MADDOCK, *Composites* **1** (1969) 104.
140. M. N. WILSON, *ibid* **1** (1970) 341.
141. M. N. WILSON, C. R. WALTERS, J. D. LEWIN and P. F. SMITH, *J. Phys. D.* **3** (1970) 1517.
142. C. R. WALTERS, *J. Phys. D.* **3** (1970) 1547.
143. M. N. WILSON and C. R. WALTERS *ibid* **3** (1970) 1547.
144. P. F. SMITH, M. N. WILSON and A. H. SPURWAY, *ibid* **3** (1970) 1561.
145. A. H. SPURWAY, J. D. LEWIN and P. F. SMITH, *ibid* **3** (1970) 1572.
146. P. S. SWARZ and C. P. BEAN, General Electric Research and Development Centre, New York, Report 68–C–039 (1968).
147. S. L. WIPF, *Phys. Rev.* **161** (1967) 404.
148. P. F. CHESTER, Proceedings of the 1st Cryogenic Engineering Conference, 9–13 April (1967) Tokyo and Kyoto, Japan (Heywood-Temple, London, 1968), pp. 147–149.
149. P. F. CHESTER, *Repts. Prog. Phys.* **30** Part II (1967) 561.
150. H. R. HART, Proceedings of Summer Study on Superconducting Devices and Accelerators, 10 June–19 July (1968) Brookhaven National Laboratory (Brookhaven National Laboratory, Upton, New York, 1969) pp. 571–600.
151. H. LONDON, *Phys. Letters* **6** (1963) 162.
152. R. HANCOX, *Proc. IEE* **113** (1966) 1221.
153. S. L. WIPF, Proceedings of Summer Study on Superconducting Devices and Accelerators, 10 June–19 July (1968) Brookhaven National Laboratory, (Brook Upton, New York, 1969) pp. 511–543.
154. A. S. YUE, Y. W. CHANG and M. P. MATHUR, Proceedings of the Conference on *In Situ* Composites, September 5–8 (1972) Lakeville, Connecticut, Vol. III (Publication NMAB 308–III, Nat. Acad. Sci., Washington, D.C. 1973) pp. 79–83.
155. A. GUINIER, C. PETIPAS, G. SAUVAGE, J. BAIXERAS, J. M. DUPART, G. FOURNET, G. FONTAINE, M. G. BLANCHIN, M. TURPIN and R. RACEK, *ibid* pp. 85–96.
156. W. A. LITTLE, *Canad. J. Phys.* **37** (1959) 334.
157. A. C. ANDERSON and R. B. RAUCH, *J. Appl. Phys.* **41** (1970) 3648.
158. K. W. GARRETT and H. M. ROSENBERG, *J. Phys. D.* **7** (1974) 1247.
159. R. E. MEREDITH and C. W. TOBIAS, *J. Appl. Phys.* **31** (1960) 1270.
160. R. L. HAMILTON and O. K. CROSSER, *Ind. Eng. Chem. Fund.* **1** (1962) 187.
161. Y. S. TOULOUKIAN, R. W. POWELL, C. Y. HO and P. G. KLEMENS, "Thermophysical Properties of Matter" Vol. 2 Thermal Conductivity – Nonmetallic Solids (IFI/Plenum, New York, 1970).
162. P. G. KLEMENS and I. N. GREENBERG, *J. Appl. Phys.* **44** (1973) 2992.
163. W. K. LIEBMANN and E. A. MILLER, *ibid* **34** (1963) 2653.

164. A. YUE, Met. Soc. AIME, Fall Meeting, Philadelphia, Pa., Oct. 1969.
165. L. M. LEVINSON, Proceedings of the Conference on *In Situ* Composites, September 5–8 (1972) Lakeville, Connecticut, Vol. III (Publication NMAB 308–III, Nat. Acad. Sci., Washington D.C. 1973) pp. 97–109.
166. C. T. ELLIOTT and S. E. R. HISCOCKS, *Brit. J. Appl. Phys. (J. Phys. D) Ser. 2* **2** (1969) 1083.
167. E. STEPHENS and E. J. EVANS, *Phil. Mag.* 7 (1929) 161.
168. N. J. STEPANOW, *Z. anorg. u. allgem. Chem.* 78 (1912) 1.
169. "Handbook of Chemistry and Physics", 49th Edn., edited by R. C. Weast (The Chemical Rubber Co. Cleveland, Ohio, 1968).

Received 10 November 1975 and accepted 1 March 1976.